S-adenosylmethionine synthases specify distinct H3K4me3 populations and gene expression patterns during heat stress

Adwait A. Godbole[1], Sneha Gopalan[2], Thien-Kim Nguyen[1], Alexander Munden[1], Paula Vo[1], Caroline A. Lewis[1], Jessica B. Spinelli[1,2], Thomas G. Fazzio[2], Amy K. Walker[1]

1. Program in Molecular Medicine, UMASS Chan Medical School, Worcester, MA 01605
2. Cancer Center, UMASS Chan Medical School, Worcester, MA 01605
3. Department of Molecular, Cell, and Cancer Biology, UMASS Chan Medical School, Worcester, MA 01605

Abstract

Methylation is a widely occurring modification that requires the methyl donor S-adenosylmethionine (SAM) and acts in regulation of gene expression and other processes. SAM is synthesized from methionine, which is imported or generated through the 1-carbon cycle (1CC). Alterations in 1CC function have clear effects on lifespan and stress responses, but the wide distribution of this modification has made identification of specific mechanistic links difficult. Exploiting a dynamic stress-induced transcription model, we find that two SAM synthases in *Caenorhabditis elegans*, SAMS-1 and SAMS-4, contribute differently to modification of H3K4me3, gene expression and survival. We find that *sams-4* enhances H3K4me3 in heat shocked animals lacking *sams-1*, however, *sams-1* cannot compensate for *sams-4*, which is required to survive heat stress. This suggests that the regulatory functions of SAM depend on its enzymatic source and that provisioning of SAM may be an important regulatory step linking 1CC function to phenotypes in aging and stress.

37 **Introduction**

38 The 1-Carbon cycle (1CC) is a group of interconnected pathways that link essential
39 nutrients such as methionine, folate and vitamin B12 to the production of nucleotides,
40 glutathione, and S-adenosylmethionine (SAM), the major methyl donor [1] (**Fig1A**). SAM
41 is important for the production of polyamines and phosphatidylcholine (PC), a
42 methylated phospholipid, and is also essential for the methylation of RNA, DNA and
43 proteins such as histones [2]. Thus, 1CC connects nutrients with the production of a key
44 cellular regulator of epigenetic function, SAM.

45

46 Alterations in 1CC function can cause a variety of defects [1], including intriguing
47 connections between this cycle, stress responses and aging. Lifespan lengthens in
48 yeast, *C. elegans*, *Drosophila* and rodent models when methionine is restricted, genes
49 in the methionine-SAM (Met-SAM) cycle are mutated, or polyamines are supplemented
50 [3]. While multiple aspects of 1CC function could affect aging, the Met-SAM cycle has
51 particularly strong links. For example, a *C. elegans* SAM synthase, *sams-1*, was
52 identified in a screen for long-lived animals [4] and multiple SAM-utilizing histone
53 methyltransferases are also implicated as aging regulators [5–7]. Of bioactive molecules,
54 SAM is second only to ATP in cellular abundance [8], which raises the question of how
55 such an abundant metabolite can exert specific phenotypic effects. Strikingly, studies in
56 multiple organisms from a variety of labs have shown that reduction in SAM levels
57 preferentially affects H3K4me3 levels [9–12]. However, changes in SAM production may
58 affect other histone modifications as well. For example, the Gasser lab showed that
59 *sams-1* and *sams-3* have distinct roles in heterochromatin formation, which involves

60 H3K9me3 [13] A yeast SAM synthase has also been shown to act as part of the SESAME
61 histone modification complex [14] or to cooperate with the SIN3 repressor [15]. In addition,
62 most eukaryotes have more than one SAM synthase, which could allow partitioning of
63 enzyme output by developmental stage, tissue type or cellular process and underlie
64 specific phenotypic effects. Indeed, in budding yeast, SAM1 and SAM2 are co-
65 expressed but regulated by different metabolic events, have distinct posttranslational
66 modifications, and act differently in phenotypes such as genome stability [16]. The two
67 SAM synthases present in mammals are expressed in distinct tissues: MAT2A is
68 present throughout development and in most adult tissues, whereas MAT1A is specific
69 to adult liver [17]. MAT2A may be present in distinct regulatory conformations with its
70 partner MAT2B [17]. However, the distinct molecular mechanisms impacted by these
71 synthases are less clear. Studies exploring specificity of metazoan SAM synthase
72 function have been difficult, as MAT1A expression decreases *ex vivo* and MAT2A is
73 essential for cell viability [18]. Finally, the high methionine content of traditional cell
74 culture media has limited functional studies [19].
75
76 We have explored SAM synthase function in *C. elegans*, where the gene family has
77 undergone an expansion. In *C. elegans*, genetic and molecular assays allow separation
78 of SAM synthase expression and function *in vivo*. Furthermore, no single SAM
79 synthase is required for survival in normal laboratory conditions or diets. *sams-1* and
80 the highly similar *sams-3*/*sams-4* are expressed in adult animals, whereas *sams-5* is
81 present at low levels in adults and *sams-2* is a pseudogene [20]. We previously found
82 that *sams-1* had multiple distinct functions, contributing to PC pools and stimulating lipid

synthesis through a feedback loop involving *sbp-1*/SREBP-1 [21] as well as regulating global H3K4me3 levels in intestinal nuclei [12]. Our studies also showed that loss of *sams-1* produced different phenotypes in bacterial or heat stress. While *sams-1* was necessary for pathogen challenge, promoter H3K4me3 and expression of immune genes, animals surprisingly survived better during heat shock when they lacked *sams-1* [12]. Because heat shocked animals require the H3K4me3 methyltransferase *set-16/MLL* for survival, we hypothesized that SAM from a different source may be important for histone methylation and survival in the heat shock response. Here, we find that SAM source impacts the functional outputs of methylation. While the SAM and the 1CC are well associated with regulation of lifespan and stress responses, direct molecular connections have been difficult to discover. Mechanisms controlling provisioning of SAM, therefore, could provide a critical level of regulation in these processes. We show that *sams-1* and *sams-4* differentially affect different populations of histone methylation and thus gene expression in the heat shock response, and that their loss results in opposing phenotypes. Our study demonstrates that SAM synthases have a critical impact on distinct methylation targets and phenotypes associated with the stress response. Thus, defining the specificity of SAM synthases may provide a method to identify from broad effects methylation events that are specific phenotypic drivers.

106 ## Results

107 ***sams-1* and *sams-4* have overlapping and distinct expression patterns and gene**
108 **regulatory effects**

109 Animals respond to stress by activating specialized protective gene expression
110 programs [22]. While these programs depend on specific signaling and transcriptional
111 activators, they may also be impacted by histone methylation and the production of
112 SAM. For example, we found that *C. elegans* lacking *sams-1* die rapidly on pathogenic
113 bacteria, have low global H3K4me3 and fail to upregulate immune response genes [12].
114 In contrast, heat shocked animals survive better without *sams-1*[23]. *sams-1(RNAi)*
115 animals induced heat shock genes to normal levels and acquired additional changes in
116 the transcriptome, including downregulation of many metabolic genes. However, the
117 H3K4me3 methyltransferase *set-16*/MLL was essential for survival [23], suggesting that
118 methylation was required. We hypothesized that other SAM synthases could play an
119 important role in mediating survival during heat shock (**Fig1A**).
120

121 In order to test these hypotheses, we first compared expression of each synthase, SAM
122 levels and gene expression after RNAi in adult unstressed animals. ModEncode data[24]
123 from young adult animals shows that in young adult levels, *sams-1* is expressed at the
124 highest levels, comparable to the metabolic enzyme GAPDH (*gpdh-1*) (**FigS1A**). *sams-*
125 *3* and *sams-4* are expressed at lower levels, but comparable to other enzymes of the 1-
126 Carbon cycle such as *metr-1*, whereas *sams-5* is minimally expressed (**FigS1A**). In
127 order to determine the tissue-specific patterns of the SAM synthases expressed in adult
128 animals, we obtained strains where each protein was tagged with RFP, GFP or mKate,

129 via CRISPR (**Fig1B, FigS1B, C**). RFP::*sams-1* and GFP::*sams-4* animals were also
130 crossed to allow visualize expression of both synthases (**Fig1B**). RFP::SAMS-
131 1fluorescence was evident in much of the adult animal, including intestine, hypodermis
132 and cells in the head (**Fig1B, FigS1B**), in line with mRNA expression patterns derived
133 from tissue-specific RNA seq [25]. However, RFP::SAMS-1was not present in the
134 germline, which did express GFP::SAMS-4 and SAMS-3::mKate (**Fig1B, S1C**).
135 GFP::SAMS-4 and SAMS-3::mKate was also present in intestinal and hypodermal cells
136 (**Fig1B, FigS1C**), demonstrating that these tissues, which are major contributors to the
137 stress response [26] contain each of these SAM synthases. *sams-3* and *sams-4* are
138 expressed bidirectionally from the same promoter and share 95% sequence identity at
139 the nucleotide level thus RNAi targeting is likely to affect both genes. Indeed SAMS-
140 3::mKate and GFP::SAMS-4 were reduced after either RNAi (**FigS1C**). Next, we used
141 mass spectrometry to compare SAM levels after *sams-3* and *sams-4* RNAi and found
142 that like *sams-1*[12,21], reduction in any synthase significantly reduced but did not
143 eliminate SAM (**Fig S1D**).
144
145 In order to compare gene expression after RNA of each SAM synthase in basal
146 conditions, we used RNA sequencing (RNAseq). Principal component analysis showed
147 that *sams-1(RNAi)* and *sams-5* formed distinct clusters on the first two principal
148 components, however *sams-3* and *sams-4* were overlapping (**FigS2; Table S1: Tabs**
149 **A-C**). About half of the genes upregulated after *sams-4* knockdown also increased in
150 *sams-1(RNAi)* animals (**FigS3B).** To determine if genes related to distinct biological
151 processes were present, we compared genes upregulated after *sams-1* RNAi[23] with

152 those changing in *sams-4* RNAi with WormCat [27], which provides enrichment scores for
153 three category levels (Cat1, Cat2, Cat3) for broad to more specific comparisons.
154 WormCat finds that gene function categories at the Cat1 and Cat 2 level, such as
155 METABOLISM: Lipid (**FigS2C**) or STRESS RESPONSE: Pathogen (**FigS2D-F**), are
156 enriched at lower levels and contain different genes in *sams-4(RNAi)* animals (**Table**
157 **S1: Tabs D-F**). Notably, *fat-7* and other lipid synthesis genes that respond to low PC in
158 *sams-1* animals are not upregulated after *sams-4(RNAi)* (**TableS1:Tab:B**). These
159 findings strengthen the idea that these SAM synthases could have distinct functions.
160

161 **Opposing roles and requirements for *sams-1* and *sams-4* in the heat shock**
162 **response**

163 In order to determine if other SAM synthases expressed in adult animals contributed to
164 survival in heat shock, we compared the heat shock survival phenotypes of *C. elegans*
165 with deletions in *sams-1*, *sams-3* and *sams-4* to avoid effects of co-targeting by RNAi.
166 *sams-1(ok3033)* has a deletion covering the majority of the open reading frame and
167 extracts from these animals lack SAMS-1 protein in immunoblots[12], therefore we refer to
168 this allele as *sams-1(lof)*. *sams-4(ok3315)* animals have a deletion that removes
169 around a third of the open reading frame. Strikingly, *sams-4(ok3315)* mutants had the
170 opposite phenotype from *sams-1(lof)*, and died rapidly after heat shock (**Fig1C, D,**
171 **Table S2:Tabs B, C**). *sams-3(2932)* harbors a deletion removing most of the ORF, but
172 in contrast to *sams-4* and *sams-1,* is indistinguishable from wild type animals in a heat
173 shock response (**FigS3B**). Although *sams-3* may be co-targeted in RNAi experiments,
174 we will refer solely to *sams-4* in our discussion because it has the most direct link to the

175 heat shock phenotypes. Finally, *sams-4(RNAi)* phenotypes in the heat stress response
176 were not linked to a general failure to thrive, as *sams-4(RNAi)* animals under basal
177 conditions had modestly enhanced lifespan (**FigS3C; Table S2: Tab A**).
178
179 Next, we used immunostaining to compare global levels of H3K4me3 in *sams-1* and
180 *sams-4* RNAi nuclei during heat shock. In contrast to the reduction in H3K4me3 in
181 basal conditions in *sams-1(lof), sams-4(ok 3315)* or RNAi animals (**Fig1E-F, H-I**), we
182 detected robust levels of H3K4me3 in *sams-1(lof)* nuclei after heat shock (2 hours at
183 37°C) (**Fig1E, H**), suggesting that *sams-1*-independent mechanisms act on H3K4me3
184 during heat shock. These increases in H3K4me3 did not appear in heat shocked *sams-*
185 *4(RNAi)* intestinal nuclei (**Fig1F, I**), raising the possibility that *sams-4* contributed to the
186 effects in *sams-1(lof)* animals. Next, we wanted to test effects of reducing both *sams-1*
187 and *sams-4* levels on H3K4me3 during heat shock. Loss of multiple SAM synthases
188 reduces viability in *C. elegans* [13]. In order to circumvent this, we used dietary choline to
189 rescue PC synthesis and growth of *sams-1(RNAi)* or *(lof)* animals during development
190 [12,21]. *sams-1(lof); sams-4(RNAi)* animals were raised on choline until the L4 stage, then
191 moved to normal media for 16 hours before heat shock. Immunostaining of *sams-1(lof);*
192 *sams-4(RNAi)* intestines showed that *sams-4* is required for the H3K4me3 in heat
193 shocked *sams-1(lof)* nuclei (**Fig1G, J**). These results were identical when we used
194 RNAi to reduce *sams-1* in *sams-4(ok3315)* animals (**FigS3E**). We also asked if *sams-4*
195 was necessary for the increased survival of *sams-1* animals after heat shock and found
196 that the survival advantage in *sams-1(RNAi)* was decreased in *sams-4(ok3315)* animals
197 (**FigS3D**). These results suggest that H3K4me3 may be remodeled during heat shock

198 with SAM from distinct synthases and that *sams-4*-dependent methylation is critical for
199 survival. Previously, it was shown that H3K4me3 deposition is independent *of sams-4*
200 in embryonic nuclei [13], however, our finding that it is broadly decreased in *sams-4(RNAi)*
201 intestinal nuclei suggests it may have important roles in H3K4 methylation in adults.
202
203 Increases in H3K4me3 have also been shown to occur in budding yeast when blocks in
204 phospholipid synthesis relieve a drain on SAM and increase levels[28], which we have
205 confirmed in *C. elegans*[23]. In order to determine if SAM levels could explain differences
206 in H3K4me3 in *sams-1* and *sams-4* animals during heat shock, we used targeted
207 LC/MS to compare SAM, it's precursor methionine and S-adenosylhomocysteine (SAH),
208 the product after methyl transfer, before and after heat shock. As in our previous
209 assays, SAM decreased significantly after *sams-1* or *sams-4(RNAi)* in basal conditions
210 (**FigS3F**), whereas SAM levels increased in each population as *sams-1* or *sams-4*
211 animals were shifted to 37°C for 2 hours (**FigS3F**). Levels of methionine and SAH also
212 decreased when comparing control, *sams-1* or *sams-4(RNAi)* animals in basal vs heat
213 shocked conditions (**FigS3G, H**), consistent with increased production and utilization of
214 SAM. The increase in SAM in heat shocked animals is consistent with our data
215 showing the contribution of SAMS-4 to H3K4me3 and survival in heat shocked *sams-1*
216 animals, however, a reduction in demand for SAM if other metabolic processes are
217 reduced after heat shock could also contribute. Finally, levels of SAM in heat shocked
218 *sams-4(RNAi)* animals also rise to levels comparable to control animals at basal
219 temperatures, however, H3K4me3 remains low in these conditions.
220

221 **Histone methyltransferase and histone demethylation machinery have modest,**
222 **separable effects on *sams* mutant heat shock phenotypes**

223 SAM is necessary for histone methylation; however, histone methylation dynamics are
224 also influenced by methyltransferase (KMT) or demethylase (KDMT) activity [29].
225 Therefore, changes in histone methylation dynamics could also impact H3K4me3
226 patterns during heat shock. H3K4me3 is catalyzed by multiple versions of the
227 COMPASS complex, which each consist of one of several SET domain histone
228 methyltransferases and several shared accessory subunits [30]. In mammals, seven
229 methyltransferases in the SET1, MLL or THX groups can methylate H3K4. *C. elegans*
230 contain single orthologs from two of these groups: *set-2/*SET1 and *set-16*/MLL,
231 respectively, with roles in embryonic development [31–33], lipid accumulation and
232 transgenerational inheritance [6,7]. In adult *C. elegans*, *set-2* RNAi results in extensive
233 loss of H3K4me3 in intestinal nuclei and although *set-16(RNAi)* causes an intermediate
234 reduction in bulk H3K4me3 levels, it has a broader requirement for survival during
235 stress [23]. Because specificity for H3K4 mono, di or trimethylation has not been verified
236 on a genome-wide scale for KDMTs, we examined multiple members of the H3K4 KDM
237 family.
238

239 In order to determine if KMTs or KDMT dynamics played a role in the change of
240 H3K4me3 during heat shock, we used RNAi to deplete them in *sams-1(lof)* or *sams-*
241 *4(ok3315)* animals and measured survival after heat shock and intestinal H3K4me3
242 levels. RNAi of *set-2/SET1* (**Fig2A**) or *set-16/MLL* (**Fig2B**) increased survival in *sams-*
243 *1(lof)* animals after heat shock (also **Table S2:Tabs:C, E**) and did not limit heat shock-

244 induced H3K4me3 in *sams-1(RNAi)* nuclei (**FigS4A, B**). RNAi of two KDMTs, *rbr-2*
245 (**Fig2C**) and *spr-5* (**Fig2D**) had opposite effects from the KMTs, moderately reducing
246 survival (**TableS2: Tab F**), whereas *amx-1* and *lsd-1* had no effect (**FigS4G, H;**
247 **TableS2: Tabs I, J**). RNAi of *set-2* (**Fig2E**) or *set-16* (**Fig2F**) had slight, but statistically
248 significant effects, increasing survival of *sams-4(ok3315)* animals (**TableS2: Tabs G,**
249 **H**). However, survival was still significantly below controls in *sams-4(ok3315)* with or
250 without the KMT RNAi. Taken together, this suggests that *set-2* and *set-16* may act
251 redundantly in the deposition of H3K4me3 after heat shock and are important to survival
252 in *sams-1(lof)* animals. Furthermore, our data illustrate that the context is critical for
253 understanding role of SAM and H3K4me3 in stress; *sams-4* and *set-16* are generally
254 required for survival after heat shock, but loss of either H3K4 KTM enhances survival in
255 *sams-1(lof)* animals.
256

257 **Distinct patterns of H3K4me3 and gene expression in *sams-1(RNAi)* versus *sams-***
258 ***4(RNAi)* animals during heat shock**

259 H3K4me3 is a prevalent modification enriched near the transcription start sites (TSSs)
260 of actively expressed genes [34]. Differing global patterns of H3K4me3 in *sams-1(RNAi)*
261 and *sams-4(RNAi)* nuclei suggest this histone modification at specific sites could also
262 be distinct. In order to identify loci that might link H3K4me3 to these phenotypes, we
263 used CUT&Tag, (Cleavage Under Targets and Tagmentation, C&T) [35], to determine
264 genome-wide H3K4me3 levels in Control RNAi, *sams-1* and *sams-4(RNAi)* in basal
265 (15°C) and after heat shock (37°C/2 hours) from two biologically independent replicates
266 along with no antibody controls. C&T is uniquely suited to the small sample sizes

267 available from these stressed populations. In this approach, a proteinA-Tn5
268 transposase fusion protein binds to the target antibody in native chromatin and DNA
269 libraries corresponding to antibody binding sites are generated after transposase
270 activation. After sequencing of libraries, we used the HOMER analysis suite[36] to
271 analyze reads mapped to the *C. elegans* genome and called peaks using
272 ChIPSeqAnno[37] for more detailed peak annotation. Bar plots from ChIPSeqAnno
273 annotations and TSS plots generated with HOMER show robust mapping of H3K4me3
274 to promoter-TSS regions, validating this approach (**Fig3A; TableS3: Tabs A-F**). While
275 promoter-TSS regions were the largest feature in each sample, heat shocked *sams-*
276 *4(RNAi)* animals had fewer overall peaks (**Fig3A**). Correlation plots also show strong
277 similarity between replicates (**FigS5A**). Because C&T has not been extensively used in
278 *C. elegans*, we compared data from basal conditions in our study to three previously
279 published ChIP-Seq data sets[38,3940]. We compared our C&T data from wild type young
280 adult animals grown at 15°C on control RNAi food (HT115) against ModEncode (L3
281 animals), *glp-1(e2141)* mutants from Pu et al.[41] and wild type adults grown at 20°C on
282 OP50 bacteria from Wan et al. [40] by computing a pair-wise Pearson correlation. We
283 found our C&T clustered most closely with the ChiPSeq from wild type animals in Wan
284 et al., along with one of the modEndode replicates (**FigS5B**) with moderate correlation
285 scores. Both our C&T data and the Wan ChiPseq data correlated poorly with the Pu et
286 al. ChIP seq, which is likely due to the lack of germline nuclei in these animals. The
287 moderate correlation between our data and ChiP seq from Wan et al may be due to
288 differences in growth temperature and bacterial diet. As a part of our quality control, we
289 visually inspected browser tracks around the *pcaf-1* gene, which is a long gene and has

290 been used by our labs and others as a positive control for H3K4me3 localization in the 5
291 prime regions [12,32]. H3K4me3 peaks are prominent upstream of the transcript as
292 expected and the no antibody libraries showed few reads (**FigS5C**).
293
294 Next, we compared TSS distributions and examined overlap between H3K4me3 peaks
295 in Control RNAi animals in basal and heat shock conditions and found moderate
296 reductions occurred with heat shock (**Fig3B**). Around 20-30% of peaks were specific to
297 at either at basal (15°C) vs. heat shock (37°C) temperature (**Fig3C)**, suggesting that
298 H3K4me3 could be remodeled upon heat shock in *C. elegans*. TSS enrichment of
299 H3K4me3 was sharply reduced in both *sams-1* and *sams-4* samples at 15°C, however
300 this difference was less marked in heat shocked animals, in line with lower TSS
301 localization in Control animals (**Fig3D, E**). While aggregate TSS enrichment for
302 H3K4me3 was similar for *sams-1* and *sams-4* RNAi animals, this analysis could miss
303 distinct sets of H3K4me3 marked genes in each condition. Indeed, Control, *sams-1* and
304 *sams-4(RNAi)* animals each showed 500-1000 specific peaks in basal conditions, with
305 moderate increases in these numbers after heat shock (**Fig3D, E**). As H3K4me3 is a
306 widely occurring modification, we hypothesized that we might better understand
307 potential SAM synthase-specific requirements if we focused on peaks that change in the
308 Control RNAi heat shock response and asked how they are affected by loss of *sams-1*
309 or *sams-4*. We used two different methods for comparing potential SAM synthase
310 requirements for H3K4me3 in the heat shock response. First, we used differential peak
311 calling (ChIPPeakAnno [37]) followed by WormCat category enrichment to determine the
312 classes of genes which might be affected (**FigS6A-F; TableS3; Tabs G-I**). Peaks

313 present in both basal and heat shocked conditions were enriched for genes in the
314 METABOLISM category (including Lipid: phospholipid, sphingolipid, sterol and lipid
315 binding, along with mitochondrial genes) as well as in core function categories such as
316 those involved in trafficking, DNA or mRNA functions (**Fig3F, FigS6D-E; Table S3:**
317 **Tabs G-I)**. There was no significant category enrichment specific to 15°C animals, but
318 after heat shock, Control RNAi animals gain enrichment in peaks at the Category 1 level
319 in PROTEOSOME PROTEOLYSIS (**Fig3F**). This enrichment was driven by increases
320 in H3K4me3 at E3: Fbox genes (**FigS6A, B; Table S3:Tab A,B**), which could be
321 important for eliminating mis-folded proteins during heat shock. Comparison of peaks
322 differentially present in *sams-1* and *sams-4* RNAi animals showed that only *sams-*
323 *1(RNAi)* exhibited a similar enrichment to Control RNAi in the PROTEOLYSIS
324 PROTEOSOME category (**Fig3G, FigS6C, D**), which could help explain the reduced
325 survival of *sams-4(RNAi)* animals relative to *sams-1(RNAi)* animals. *sams-1* RNAi
326 animals also gained enriched peaks in a wide range of gene categories within
327 METABOLISM, whereas *sams-4(RNAi)* enriched peaks in these categories were more
328 limited (**FigS6C-F**). Thus, loss of *sams-1* or *sams-4* differentially affects H3K4me3
329 peaks within functional gene classes that also change in the heat shock response.
330
331 Next, we hypothesized that H3K4me3 at peaks in Control RNAi animals might reflect
332 multiple differently regulated populations, some which are linked to SAM synthase
333 function and others that are regulated at other levels. In order to test this, we divided
334 peaks in Control animals at 15°C or 37°C into those that did not change after SAM
335 synthase RNAi (*sams-1* or *sams-4* independent peaks) or those that were dependent on

336 *sams-1* or *sams-4* and examined aggregations around TSS regions. There was little
337 difference between TSS plots of *sams-1* or *sams-4*-independent genes at either
338 temperature (**Fig3H, I**). However, in basal conditions, Control peaks that depended on
339 *sams-1* had more marked TSS localization (**Fig3J**), demonstrating that *sams-1* and
340 *sams-4* dependent peaks have distinct TSS architectures. TSS localization was low in
341 all 37°C samples, following the general trend of decrease after heat shock (**Fig3K**). We
342 next separated Control peaks into those that were generally SAM synthase-dependent
343 and those that were specific to loss of *sams-1* or *sams-4*. Aggregation of these peaks
344 shows that peaks in Control 15°C samples that were lost only in *sams-4* RNAi also had
345 the lowest levels of H3K4me3 in TSS regions, whereas promoters that lost this
346 modification only after *sams-1* RNAi had higher levels of H3K4me3 (**FigS6G**). Control
347 37°C samples exhibited a similar pattern, with a lower H3K4me3 level overall consistent
348 with what we have observed in heat shock samples (**FigS6H**). Thus, genome wide
349 H3K4me3 contain multiple populations with distinct TSS patterns. Peaks that are
350 present even when *sams-1* or *sams-4* are depleted have the highest levels, whereas
351 *sams-1*-dependent peaks have moderate H3K4me3, and peaks that are lost after *sams-*
352 *4* RNAi have the lowest levels. Taken together, this shows that individual SAM
353 synthases are linked to distinct sets of H3K4me3 within the genome.
354

355 **RNAi of *sams-1* or *sams-4* has similar effects on TSS peaks at tissue-specific**
356 **genes**

357 Our C&T and RNA seq assays were performed on whole animals. While *sams-1* and
358 *sams-4* are co-expressed in the intestine and hypodermis, which are major stress-

359 responsive tissues, the germline nuclei contain only *sams-4* (**Fig1B** and **FigS1B**). This
360 aligns with our previous observations that *sams-1(RNAi)* animals had normal patterns of
361 H3K4me3 in germline nuclei (Ding, et al. 2015), whereas RNAi of *sams-4* abrogates
362 H3K4me3 staining in germline nuclei (**FigS7A**). However, embryo production and
363 development appear broadly normal in *sams-4* RNAi embryos (not shown). In order to
364 determine how H3K4me3 might align with tissue-specific expression patterns, we
365 aggregated peaks from tissue-specific RNA seq data published by Serizay, et al [42].
366 Serizay et al. separated nuclei based on tissue specific GFP expression and defined
367 gene sets that were expressed that were ubiquitously, as well as those that were
368 present only in a single tissue. They also performed ATAC seq (Assay for
369 Transposase-Accessible Chromatin using sequencing). Serizay, et al. defined
370 transcripts by expression pattern and defined sets that were specific to (*tissue*_only), or
371 represented in across multiple tissues (*tissue*_all). ubiquitious_all and Germline_only
372 genes had the most defined patterns of open chromatin around TSSs [42] We compared
373 our C&T data with Ubiquitious_all, Germline_only and Intestine_only genes and found
374 that we identified peaks for around half of these genes in Control RNAi animals at 15°C
375 or 37°C (**FigS7B-D)**. We found the ubiquitous_all and germline_only genes also had
376 strong H3K4me3 peaks that were reduced equally by *sams-1* or *sams-4* RNAi in both
377 temperature conditions (**FigS7D, G; E, H**). Intestine_only genes showed lower TSS
378 enrichment but were similarly reduced after *sams-1* or *sams-4* RNAi (**FigS7H, I**). These
379 data suggest that differences in germline expression for *sams-1* and *sams-4* are not
380 sufficient to explain differential effects on H3K4me3 peak populations.
381

382 **Poor expression of heat shock gene suite in *sams-4(RNAi)* animals**

383 H3K4me3 is found at the promoters of many actively transcribed genes, but it is not
384 necessarily required for gene expression [29]. However, studying chromatin modification
385 in stress responses may reveal additional regulatory effects [43]. We previously found
386 using ChIP-PCR in the context of the stress response in *C. elegans* that H3K4me3
387 increased at promoters of genes that responded to bacterial stress in a *sams-1-*
388 dependent manner[12]. However, during the stress response, H3K4me3 did not change
389 at multiple non-stress responsive genes, suggesting that stress-responsive loci might be
390 more sensitive to SAM levels[12]. In order to identify genes that changed in SAM-
391 deficient animals, we performed RNA seq, then compared genes induced by heat shock
392 in control and *sams-1(RNAi)*[23] with genes induced in *sams-4(RNAi)* animals **(TableS4:**
393 **A-C**). Upregulated genes for control and *sams-1(RNAi)* animals appeared closely
394 grouped in principal component analysis, with sams-4(RNAi) upregulated genes and all
395 downregulated gene sets forming distinct groups (**FigS8A**). We previously noted that
396 while *sams-1(RNAi)* animals could not mount the full transcriptional response to
397 bacterial stress, most genes activated by heat increased similarly to controls[23]. *sams-*
398 *4(RNAi)* animals, in contrast, activate less than 25% of the genes induced by heat in
399 control animals (**Fig4A**). *sams-1(RNAi)* and *sams-4(RNAi)* animals also induce more
400 that 600 genes in response to heat that are SAM-synthase-specific and which do not
401 increase in control animals (**Fig4A**). WormCat pathway analysis shows that *sams-*
402 *4(RNAi)* animals lack the robust enrichment in STRESS RESPONSE (Cat1) and
403 STRESS RESPONSE: Heat (Cat2) evidenced in both Control and *sams-1(RNAi)*
404 samples (**Fig4B; TableS4: D-F**). In addition, enrichment of the CHAPERONE,

405 PROTEOLYSIS PROTEOSOME categories occurring in *sams-1(RNAi)* animals does
406 not occur after *sams-4(RNAi)*, reflecting lack of induction of these genes which could be
407 important for proteostasis in the heat shock response (**Fig4C**). Thus, reduction in
408 *sams-1* or *sams-4* results in distinct gene expression programs in both basal conditions
409 (**FigS2A-F**) and during the heat stress response (**Fig4A-C**). This differentiation of gene
410 expression programs clearly shows that *sams-1* and *sams-4* have distinct functional
411 roles.
412
413 Gene expression changes occurring after *sams-1* or *sams-4* depletion could result from
414 direct effects on H3K4me3 or other potential methylation targets, or from indirect
415 effects. Evaluating the impact H3K4me3 on gene expression is also complex, as this
416 modification is generally associated but not necessary for expression of actively
417 transcribed genes [29]. In our analysis of H3K4me3 peaks during the heat stress
418 response, we found evidence of multiple peak populations that depend on or occur
419 independently of *sams-1* or *sams-4* (**Fig2H-K, FigS6A-F**). We reasoned, therefore, that
420 it was also critical to determine H3K4me3 levels at *sams-1-* or *sams-4*-dependent genes
421 in the heat shock response.
422
423 First, we examined H3K4me3 peak levels at genes with increased in Control RNAi,
424 *sams-1(RNAi)* or *sams-4(RNAi)* during heat shock. We found that genes dependent on
425 *sams-1* or *sams-4* in the heat shock response were marked by lower overall H3K4me3
426 levels at the TSSs (**Fig4D**). However, this analysis included large numbers of
427 upregulated genes in *sams-1* or *sams-4* outside of the wildtype heat stress response.

428 Therefore, we next focused on genes normally upregulated during heat shock and
429 divided them according to SAM synthase dependence. Strikingly, isolating the *sams-1*-
430 dependent genes revealed a strong peak 5' to the TSS, which was not evident in the
431 larger subset of Control or *sams-4(RNAi)*-dependent upregulated genes (**Fig4E, F**).
432 Among the genes with robust peaks in heat shocked *sams-1(RNAi)* animals were two F-
433 box proteins, *fbxa-59* and T27F6.8, which were robustly expressed in *sams-1* but not
434 *sams-4* animals (**Fig4C, G-I**). Down regulation of T27F6.8 did not affect the survival of
435 the animals after heat shock (**FigS8B**) while survival of animals fed *fbxa-59* RNAi was
436 modestly affected (**FigS8C**). Survival in heat shock may be multi-genic and rely on
437 pathway responses rather than single genes. However, our data reveals genes
438 upregulated in the heat shock response may have different H3K4me3 levels depending
439 on requirements for *sams-1* or *sams-4*. In addition, our results suggest that roles for
440 H3K4me3 may become clearer when genome-wide methylation populations are
441 separated into biologically responsive categories.
442

443 **SAM synthase-specific effects on genes downregulated in the heat shock**
444 **response**

445 Transcriptional responses to heat shock largely focus on rapidly induced genes that
446 provide protection from changes in proteostasis [44,45]. However, downregulated genes
447 could also play important roles. For example, the WormCat category of
448 TRANSMEMBRANE TRANSPORT (TM TRANS) is enriched in genes downregulated
449 after heat shock in *C. elegans* (**Fig5A, B**). Previously we observed that heat shocked
450 animals depended on *sams-1* for normal expression of nearly 2,000 genes, falling within

451 WormCat Categories of METABOLISM, TRANSCRIPTION FACTOR (TF),
452 SIGNALLING and STRESS RESPONSE[23] (**Fig5A, B**). Interestingly, the metabolic
453 genes dependent on *sams-1* include those in lipid metabolism, whereas the TF
454 enrichment was centered around nuclear hormone receptors (NHRs) (**Fig5C, D**), which
455 regulate many metabolic and stress responsive genes in *C. elegans* [46]. However,
456 neither the shared TM TRANSPORT nor the *sams-1* specific categories depend on
457 *sams-4* (**Fig5B, C**). Thus, as in genes upregulated during the heat shock response,
458 genes downregulated in the heat shock response also have differential requirements for
459 *sams-1* and *sams-4*.
460
461 Next, we examined H3K4me3 levels around TSSs of genes that lost expression during
462 heat shock in Control, *sams-1* or *sams-4(RNAi)* animals. Genes decreasing in Control
463 animals had a slight reduction of H3K4me3 peaks when comparing15°C and 37°C
464 samples, consistent with global levels after heat shock (**Fig5D**). RNAi of *sams-1 or*
465 *sams-4* also broadly reduced H3K4me3 TSS enrichment at downregulated genes
466 (**Fig5D-F**). However, there were minimal differences before or after heat shock,
467 suggesting expression patterns affecting survival could be established before induction
468 of the stress.
469
470 H3K4me3 has been reported to act as a bookmarking modification, therefore we
471 hypothesized that some loci could be affected before heat shock, with expression
472 changing afterward. Therefore, we more closely examined genes with *sams-1*-
473 dependent H3K4me3 at 15°C that lost expression during heat shock. Those genes

474 were highly enriched for METABOLISM: Lipid: beta oxidation and NHR transcription
475 factors (**Fig6A**). We noted they included multiple members of a regulatory circuit that
476 control expression of a beta-oxidation-like pathway that degrades toxic fatty acids
477 identified by the Walhout lab [47], including *nhr-68*, *nhr-114* and beta-oxidation genes
478 *acdh-1, hach-1 ech-6, -8,* and *-9* **(Fig6B, C**). Indeed, *nhr-68*, the initiating TF in this
479 regulatory circuit, shows lower levels of H3K4me3 at its promoter in basal conditions,
480 compared to Control or *sams-4* RNAi animals (**Fig6D**). The H3K4me3 peak overlaps
481 with another gene, *pms-2*, whose expression does not change after heat shock or upon
482 SAM synthase RNAi (**TableS4: Tabs A-C**). In order to test if H3K4me3-dependent
483 regulation of *nhr-68* was important for survival during heat shock, we made use of a
484 construct expressing *nhr-68* under the intestine-specific *ges-1* promoter[47], where
485 H3K4me3 peaks do not change after RNAi of *sams-1* or *sams-4* (**FigS9A**). Expression
486 of *nhr-68* under this heterologous promoter had a moderate, but significant effect on
487 survival (**Fig6E**). Thus, downregulation of *nhr-68* in sams-1 animals after heat shock
488 could be part of a program enhancing survival. Taken together, our results suggest
489 differences in H3K4me3 patterns in *sams-1* and *sams-4* animals before heat shock may
490 also influence gene expression patterns during the stress response. This demonstrates
491 that *sams-1* and *sams-4* are required for distinct sets of genes in the heat stress
492 response and contribute to different H3K4me3 patterns.
493
494
495

496 **Discussion**

497 The molecules that modify chromatin are produced by metabolic pathways [48]. Use of
498 ATP, AcetylCoA or SAM for phosphorylation, acetylation or methylation of histones is
499 tightly regulated and many studies have focused on control of enzymes or enzyme-
500 containing complexes. Acetylation and methylation may also be regulated by
501 metabolite levels [49,50]. This allows the chromatin environment to sense and respond to
502 changes in key metabolic pathways. However, effects of methylation on chromatin are
503 multifaceted: DNA and H3K9me9 have strong repressive effects, whereas other
504 modifications such as H3K4me3 and H3K36me3 are associated with active transcription
505 [29]. These marks, especially H3K4me3, are most sensitive to SAM levels, most likely
506 due to the kinetics of the H3K4me3 MTs [51]. SAM is an abundant metabolite that
507 contributes to multiple biosynthetic pathways in addition to acting as the major donor for
508 histone, DNA and RNA methylation [52]. Reduction in SAM levels has major phenotypic
509 consequences in animals, altering lipid levels in murine liver and *C. elegans* [21,53],
510 altering differentiation potential in iPS cells [10] and changing stress resistance [23]. In
511 addition, 1CC has been identified as a causal regulator of aging [54] and is important in
512 cancer development [19,55]. However, the abundance of SAM and its targets have made
513 it difficult to connect changes in methylation to molecular pathways regulating these
514 physiological effects. In addition, studying effects of SAM is difficult in culture because
515 SAM itself is labile [56] and tissue culture media is replete with 1CC metabolites [19].
516 Important insights have been made into the impact of SAM on the breadth of H3K4me3
517 peaks using methionine depletion [9,57,58], however, this approach could affect other
518 pathways. In this study, we have taken the approach of limiting SAM synthase

519 expression in *C. elegans*, then using genetic and molecular approaches to link
520 methylation-dependent pathways to changes in stress responses. We found that
521 individual SAM synthases could have distinct effects even on a single methylation target
522 such as H3K4me3. This observation not only shows that examining how SAM is
523 produced within the cells allows differentiation of phenotypic effects, but also supports
524 the striking notion of 'where' SAM comes from affects its functional output. While
525 mammalian cells express either one of two SAM synthases, MAT2A, which is present in
526 non-liver cells, may be present in multiple regulatory isoforms [59]. Thus, the isoform-
527 specific production and functional targets for SAM synthases we uncover could also be
528 important in mammals. Hints of this exist in other cellular systems – 1CC enzymes, for
529 example, have been associated with chromatin modifying complex in yeast [14] and
530 mammalian cells [60].
531
532 H3K4me3 is clearly an important link between SAM levels, aging and stress
533 phenotypes, as loss or reduction of H3K4 MT function phenocopy aspects of SAM
534 depletion [12,23]. However, this modification is also wide-spread, and transcription may
535 occur even when this mark is not present [61]. By studying acute changes in gene
536 expression during heat stress response in *C. elegans*, we have found that H3K4me3
537 populations can also be separated based on SAM synthase requirements. The
538 importance of H3K4me3 during heat shock is also reflected in the interactions between
539 the SAM synthases and the KMTs/KDMTs as lowering levels of *set-2* or *set-16* increase
540 survival. This suggests that the context of low SAM from SAMS-1, reducing H3K4me3

541 can have additional benefits. Future studies identifying genomic targets of H3K4me3
542 KMTs together with SAM synthases may be important for untangling these effects.
543
544 SAM synthase-specific effects may also vary according to the biological context, as loss
545 of *sams-1* improves the ability of *C. elegans* to survive heat stress, while limiting its
546 ability to withstand bacterial pathogens [23]. Our previous studies showed that the
547 induction of bacterial pathogen induced genes was limited in the absence of *sams-1*,
548 however, in this study, we find links between *sams-1*-dependent genes in basal
549 conditions and effects on survival after heat shock. Thus, the altered methylation
550 landscape in *sams-1* animals provides a context favorable to extended lifespan and
551 survival in heat stress but which limits other stress responsive genes. This context may
552 depend on systems level effects and not on a single "target" gene, as our analysis of
553 genes that lose peaks in *sams-1* or *sams-4(RNAi)* animals have modest effects, but do
554 not recapitulate the entire phenotype. It is also possible that there are genes or specific
555 modules that drive enhanced survival in *sams-1* animal or responsible for viability after
556 loss of *sams-4(RNAi)*. Our approach dividing peaks into groups based on
557 responsiveness to *sams-1* or *sams-4* demonstrates the importance of identifying
558 specific populations of H3K4me3; combining *set-2* or *set-16* sensitive loci may provide
559 the resolution to identify these loci in future studies. Manipulation of the 1CC is of
560 interest as a modulator of aging[54] and affects multiple biological processes. Our studies
561 demonstrate that lowering SAM, or reducing levels of a key methylation target such as
562 H3K4me3, does not represent a single biological state and that it is important to
563 consider that effects may depend on synthase-specific regulation or context. Future

identification of these regulators will provide the mechanistic details key to understanding the role of the 1CC in aging and stress.

Limitations:

The genetic tools used in our study provide a method to reduce SAM from a specific enzymatic source. However, the roles for SAM in the cell are broad and can affect methylation of multiple targets. While our metabolomics assays show that SAM increases in heat shocked *sams-1(RNAi)* animals, we have not demonstrated that this SAM is derived from *sams-4*. In addition, survival benefits after heat shock occur across broad cellular functions including proteostasis and other methylation marks such as H3K9me3 [62]. Thus, there may be multiple additional methylation-dependent mechanisms that influence survival of *sams-1* or *sams-4* animals during heat shock. In addition, we measured gene expression and H3K4me3 at two hours post heat shock, whereas the survival assay occurs over multiple days. Thus, there may be changes in gene expression or histone modifications occurring at later times that also affect survival.

581 **Materials and methods**

582 ***C. elegans strains***

583 N2(Caenorhabditis Genetics Center); *sams-1(lof)(ok3033)*; *sams-3(ok2932) IV*, *sams-*
584 *4((ok3315)* IV, Caenorhabditis Genetics Center), tagRFP::SAMS-1 (WAL500, this
585 study); GFP::SAM-4(WALK501, this study); SAMS-1::RFP;GFP::SAMS-4(WAL502, this
586 study), SAMS-3::mKate (WAL305). *Pges-1*::NHR-68::GFP (VL1296)[47]. CRISPR
587 tagging for WAL500 and WAL501 were done by the UMASS Medical School transgenic
588 core, confirmed by PCR for genotype and outcrossed three times to wild type animals.
589 Next, each strain was crossed to the respective deletion allele to create WAL503
590 (RFP::*sams-1(ker5); sams-1(ok3033)*) and WAL504(GFP::*sams-4(ker6); sams-*
591 *4(ok3315)*). *sams-3::mKate(nu3139)* (COP2476) was constructed using CRISPR by In
592 Vivo biosystems then outcrossed 3 times (WAL305).

593

594 ***C. elegans* culture, RNAi and stress applications.**

595 *C. elegans* (N2) were cultured using standard laboratory conditions on *E. coli* OP50 or
596 HT115 expressing appropriate RNAi. RNAi expression was induced using 6 mM IPTG.
597 Adults were bleached onto RNAi plates and allowed to develop to the L4 to young adult
598 transition before stresses were applied. For heat stress applications, animals were
599 raised at 15°C from hatching then at the L4/young adult transition replicate plates were
600 placed at 15°C or 37°C for 2 hours. After each stress, animals were washed off the
601 plates with S-basal, then pellets frozen at -80°C. RNA was prepared as in[12]. For
602 survival assays, ~10 -15 adult N2 animals were bleached on 60 mm RNAi plates. The
603 eggs were allowed to hatch and grow to young adults at 15ºC. 25-30 young adults were

604 then moved to 35 mm plates in triplicate (75-90 animals per RNAi treatment) and
605 subjected to heat shock at 37°C for 2 hours. Animals were kept at 20°C for the
606 remainder of the assay. Dead animals were identified by gentle prodding, were counted
607 and removed each day. Animals that died of bagging or from desiccation on the side of
608 the plate were not counted. Three independent non blinded biological replicates were
609 carried out and Kaplan-Meir curves were generated with GraphPad Prism v8.0. For
610 lifespan experiments, the N2 adults were bleached on 60 mm RNAi plates. The eggs
611 were allowed to hatch and grow to young adults at 20°C. 25-30 young adults were then
612 moved to 35 mm plates in triplicate (75-90 animals per RNAi treatment). Adults were
613 moved to fresh plates every day and dead animals were identified by gentle prodding
614 and removed each day. Three independent non blinded biological replicates were
615 carried out and Kaplan-Meir curves were generated with GraphPad Prism v8.0.
616

617 **Gene expression analysis, RNA sequencing and analysis**

618 RNA for deep sequencing was purified by Qiagen RNAeasy. Duplicate samples were
619 sent for library construction and sequencing at BGI (China). Raw sequencing reads
620 were processed using an in-house RNA-Seq data processing software Dolphin at
621 University of Massachusetts Medical School [63]. The raw read pairs were first aligned to
622 *C. elegans* reference genome with ws245 annotation. The RSEM method was used to
623 quantify the expression levels of genes and Deseq was used to produce differentially
624 expressed gene sets with more than a 2-fold difference in gene expression, with
625 replicates being within 0.05 in a Students T test and a False Discovery Rate (FDR)
626 under 0.01. Statistics were calculated with DeBrowser [64]. Venn Diagrams were

627 constructed by BioVenn [65]. WormCat analysis was performed using the website
628 www.wormcat.com[27,66] and the whole genome annotation version 2 (v2) and indicated
629 gene sets. PCA was conducted by using *prcomp* in R and graphed with *ggplot* in R
630 studio.
631
632 **Immunofluorescence**
633 For H3K4me3 (Cell Signaling Technology, catalogue number C42D8) staining,
634 dissected intestines were incubated in 2% paraformaldehyde, freeze cracked, then
635 treated with -20^{0}C ethanol before washing in PBS, 1% Tween-20, and 0.1% BSA.
636 Images were taken on a Leica SPE II at identical gain settings within experimental sets.
637 Quantitation was derived for pixel intensity over nuclear area for at least seven
638 dissected intestines, with at least 3 nuclei per intestine. Three biological repeats were
639 carried out for every experiment.
640
641 **Sample preparation for LC-MS**
642 *C. elegans* (N2) gravid adults (~15-20) were bleached onto 60 mm RNAi plates, eggs
643 were allowed to hatch and grow to young adults at 15°C. For heat stress application,
644 replicate plates were placed at either 15°C or 37°C for 2 hours. At the end of the heat
645 stress, worms were collected in S-Basal, and pellets were frozen at -80°C. Four
646 independent biological replicates were collected. To prepare the samples for LC-MS,
647 the pellet was thawed on ice and washed with 0.9% NaCl. Washed worms were then
648 transferred to 2 mL FASTPREP tubes (MP Biomedicals) containing 1.4 mm ceramic
649 beads (Qiagen). The samples were then resuspended in 1 mL 80% methanol (LC-MS

650 grade) and homogenized using a bead beater (6.5 m/s; 20 seconds). The samples were
651 cooled on ice between cycles. The homogenized samples were then vortexed at 4°C for
652 10 min and centrifuged at 21,000 RPM for 10 min at 4°C. The supernatant was removed
653 at dried under vacuum. The pellet was resuspended in ice cold RIPA buffer and
654 vortexed at 4°C for 10 min and centrifuged at 21,000 RPM at 4°C for 10 min. The
655 supernatant was removed and used for protein quantification using Pierce Protein BCA
656 assay kit (ThermoFisher). The protein quantification was then used to resuspend the
657 pellet for an equal input of 0.5 μg/ml of protein per sample.

658 **LC-MS analysis**

659 **Absolute quantification of SAM:**

660 Samples were extracted in 80% methanol containing 500 nM methionine-$^{13}C_5$-^{15}N
661 (Cambridge Isotope Laboratories, Inc.) as an internal standard and metabolites were
662 detected as described above. Absolute quantification of SAM was performed using an
663 external calibration curve prepared with synthetic standard, and peak areas were
664 normalized to methionine-$^{13}C_5$-^{15}N. Normalized peak areas from the standard curve
665 were fit to a quadratic log-log equation with an r^2 value of >0.995 which was then used
666 to calculate the concentration of SAM in each sample. Statistical analysis was carried
667 out for the data using GraphPad Prism (v8.0).

668

669 **Relative metabolite profiling**

670 Metabolomics was conducted on a QExactive Plus bench top orbitrap mass
671 spectrometer equipped with an Ion Max source and a HESI II probe, which was coupled
672 to a Vanquish Horizon HPLC system (Thermo Fisher Scientific, San Jose, CA). External

673 mass calibration was performed using the standard calibration mixture every 7 days.
674 Dried extracts were reconstituted in enough water to achieve a final concentration of 0.5
675 μg/ml protein per sample. 2 μL of this resuspended sample were injected onto a
676 SeQuant® ZIC®-pHILIC 150 x 2.1 mm analytical column equipped with a 2.1 x 20 mm
677 guard column (both 5 mm particle size; Millipore Sigma). Buffer A was 20 mM
678 ammonium carbonate, 0.1% ammonium hydroxide; Buffer B was acetonitrile. The
679 autosampler tray was held at 4◦C. The chromatographic gradient was run at a flow rate
680 of 0.150 mL/min as follows: 0-20 min: linear gradient from 80-20% B; 20-20.5 min: linear
681 gradient form 20-80% B; 20.5-28 min: hold at 80% B. The mass spectrometer was
682 operated in full-scan, polarity-switching mode, with the spray voltage set to 4.0 kV, the
683 heated capillary held at 320◦C, and the HESI probe held at 350◦C. The sheath gas flow
684 was set to 10 units, the auxiliary gas flow was set to 1 units, and the sweep gas flow
685 was set to 1 unit. MS data acquisition was performed in a range of *m/z* = 70–1000, with
686 the resolution set at 70,000, the AGC target at $1x10^6$, and the maximum injection time at
687 20 msec. An additional scan (*m/z* 220-700) in negative mode only was included to
688 enhance detection of nucleotides. Relative quantitation of polar metabolites was
689 performed TraceFinder 5.1 (Thermo Fisher Scientific) using a 5 ppm mass tolerance
690 and referencing an in-house library of chemical standards. Statistical analysis was
691 carried out for the data using GraphPad Prism (v8.0).
692

693 **CUT&Tag**

694 *C. elegans* (N2) were cultured using standard laboratory conditions on *E. coli* OP50.
695 Adults were bleached onto RNAi plates and allowed to develop to the L4 to young adult

696 transition before heat stress was applied. For heat stress applications, animals were
697 raised at 15°C from hatching then at the L4/young adult transition replicate plates were
698 placed at 15°C or 37°C for 2 hours. At the end of the heat stress, animals were washed
699 off the plates with S-basal, then pellets frozen at -80°C. Worm pellets were washed with
700 S-Basal to remove bacteria, then resuspended in 750 uL of chilled Nuclei Purification
701 Buffer (50 mM HEPES pH = 7.5, 40 mM NaCl, 90 mM KCl, 2 mM EDTA, 0.5 mM EGTA,
702 0.2 mM DTT, 0.5 mM PMSF, 0.5 mM spermidine, 0.1% tween 20, and cOmplete
703 proteinase inhibitor cocktail (Roche)). The suspension was then transferred to Potter-
704 Elvehjem Tissue Grinder (3 mL). The worms were ground with 2-3 cycles consisting of
705 ~45-50 strokes of the grinder. The samples were chilled on ice for ~5 minutes between
706 consecutive cycles. The lysates were passed through 100 micron filter (X3) followed by
707 40 micron (X3) (Pluriselect). The lysates were then centrifuged at 4500 RPM for 10
708 minutes at 4°C. The pellets were resuspended gently in wash buffer (1M HEPES pH
709 7.5, 5 M NaCl, 2 M spermidine). Concanavalin bead slurry (10 uL/sample) was added
710 gently to the samples and allowed to incubate at room temperature for 15 min in an
711 end-over-end rotator. The sample tubes were then transferred to a magnetic stand and
712 liquid was gently removed. The nuclei were gently resuspended in 50 uL of chilled
713 antibody buffer (8 µL 0.5 M EDTA, 6.7 µL 30% BSA in 2 mL Dig-wash buffer (400 µL
714 5% digitonin with 40 mL Wash buffer)). 1 uL anti-H3K4me3 antibody (Cell Signaling
715 Technology, catalogue number C42D8) was added to the suspension and allowed to
716 bind overnight at 4°C on a nutator shaker. Samples without any antibody added were
717 used as controls to correct for background reads and further processed per the
718 CUT&Tag protocol [67] to generate sequencing libraries. The libraries were amplified by

719 mixing 21 µL of DNA with 2µL each of (10 µM) barcoded i5 and i7 primers, using a
720 different combination for each sample. 25 µL NEBNext HiFi 2 × PCR Master mix (NEB)
721 was added, and PCR was performed using the following cycling conditions: 72 °C for
722 5 minutes (gap filling); 98 °C for 30 seconds; 17 cycles of 98 °C for 10 seconds and
723 63 °C for 30 s; final extension at 72 °C for 1 minute and hold at 4 °C. 1.1 × volume of
724 Ampure XP beads (Beckman Coulter) was incubated with libraries for 10 minutes at
725 room temperature to clean up the PCR mix. Bead bound DNA was purified by washing
726 twice with 80% ethanol and eluting in 20 µL 10 mM Tris pH 8.0. Size distribution of the
727 libraries was determined by Fragment analyzer and concentration by the KAPA Library
728 Quantification Kit before sequencing to determine the H3K4me3 landscape in basal and
729 heat stress condition in worms fed on control, *sams-1* or *sams-4* RNAi. Sequencing of
730 the prepared libraries was carried out on Illumina NextSeq 500.
731
732 **Data analysis**
733 Paired end reads from each sample were aligned to the *C. elegans* genome (ce11 with
734 ws245 annotations) using Bowtie2 [68]with the parameters -N 1 and -X 2000. Duplicate
735 reads were removed using Picard (http://broadinstitute.github.io/picard/) and the reads
736 with low quality scores (MAPQ < 10) were removed. HOMER software suite was used
737 to process the remaining mapped reads [36]. The “makeUCSCfile” command was used
738 for generating genome browser tracks. Data was normalized to library size. the
739 “findPeaks <tag directory> -style histone -o auto” command was used for calling
740 H3K4me3 peaks and the “annotatePeaks” command was used for making aggregation
741 plots. Differential peak calling was accomplished using [37]the command “. We used the

742 findOverlapsOfPeaks command in ChipSeqAnno[37] with a max gap of 1000 basepairs to
743 determine peak overlap. TSS plots were generated using HOMER [36] and Venn
744 Diagrams were constructed by BioVenn [65].
745
746 Correlation matrices were generated with deeptools version 3.5.1[69]. Multibamsummary
747 was used to compare bam files from each sample, using default values except --binSize
748 2000. This data was visualized using plotCorrelation with --removeOutliers and the
749 Pearson method. Previously published datasets were used to compare H3K4me3 Cut
750 and Tag versus previously published data sets. Young adults fed a normal diet were
751 used from Wan et al. 2022[40]. Day 2 *glp-1* adults were chosen from Pu et al[39].
752 modENCODE ChIP-seq data drew from L3 animals[38].
753
754
755
756

757

758 **Acknowledgements**

759 We would like to acknowledge the Walker lab for reading of the manuscript, Drs. Marian
760 Walhout and Craig Peterson for helpful discussions and Life Science editors for
761 manuscript assistance. Absolute quantification of SAM was carried out at the
762 Whitehead Metabolomics Core (Cambridge, MA). We thank the UMASS Transgenic
763 animal core (Dr. Paola Perrat and Dr. Michael Francis) for construction of RFP::SAMS-
764 1and GFP::SAMS-4. Funding is from NIH: 1R01AG053355 to AKW and R01HD072122
765 to TGF.

766

767 **Figure legends**

768 **Figure 1 *sams-1*-independent acquisition of H3K4me3 in heat shocked animals**

769 **(A)** Methionine intake through diet enters the 1 carbon cycle and is used by SAM
770 synthases for the synthesis of SAM which is used by methyltransferases to add methyl
771 moieties to proteins, nucleic acids and lipids. **(B)** Representative confocal images of
772 animals co-expressing RFP::SAMS-1and GFP::SAMS-4 in the germline and intestine.
773 Kaplan-Meier survival plots of *sams-1(lof)* (**C**) or *sams-4(ok3315)* (**D**) following heat
774 shock. Statistical significance is shown by Log-rank test. Each graph represents the
775 compiled data from 3 biologically independent repeats; data is compiled in Table S2.
776 Representative immunofluorescence images of intestinal nuclei stained with H3K4me3-
777 specific antibody and quantification in *sams-1(lof)* animals (**E, H**), *sams-4(RNAi)* (**F, I**) or
778 in *sams-1(lof); sams-4(RNAi)* animals (**G, J**). *sams-3* may also be targeted; see also
779 **Figure S3E**). Statistical significance was calculated using unpaired Student's t-test. ns=
780 not significant, **** = p<0.0001, *** = p<0.001. Graph represents compiled data from
781 three biologically independent repeats per condition.

782

783 **Figure 2: H3K4me3 demethylases modulate SAM synthase phenotypes**
784
785 Kaplan-Meier plots of survival assays comparing basal and heat shocked wild type (N2)
786 or *sams-1(lof)* animals grown on RNAi for the histone methyltransferases *set-2* (**A**) and
787 *set-16* (**B**), or demethylases *rbr-2* (**C**) and *spr-5* (**D**). Heat shock survival assays for
788 *sams-4(ok3315)* animals exposed to *set-2* or *set-16* RNAi are shown in **E, F**. Statistical
789 significance is shown by Log-rank test. Each graph represents compiled data from 3
790 biologically independent repeats. Data for each replicate is compiled in Table S2.

791

792 **Figure 3 H3K4me3 modifying enzymes modulate SAM synthase phenotypes**

793 **(A)** Bar graph showing the distribution of the enrichment of H3K4me3 over different
794 genomic loci in animals fed control RNAi, *sams-1(RNAi)* or *sams-4(RNAi)* at 15°C and
795 37°C. **(B)** Aggregation plots showing TSS enrichment in the H3K4me3 peaks identified
796 in animals fed control RNAi at 15°C and 37°C. The Y axis on TSS plots shows Peaks
797 per base pair of gene. **(C)** Venn diagram comparing the overlap in the H3K4me3
798 peaks identified in animals fed control RNAi at 15°C and 37°C. **(D)** Aggregation plots
799 showing TSS enrichment in the H3K4me3 peaks identified in animals fed control RNAi
800 or *sams-1(RNAi)* or *sams-4(RNAi)* at 15°C and Venn diagram comparing the overlap in
801 the H3K4me3 peaks identified in animals fed control RNAi or *sams-1(RNAi)* or *sams-*
802 *4(RNAi)* at 15°C. **(E)** Aggregation plots showing TSS enrichment in the H3K4me3 peaks
803 identified in animals fed control RNAi or *sams-1(RNAi)* or *sams-4(RNAi)* at 15°C and
804 Venn diagram comparing the overlap in the H3K4me3 peaks identified in animals fed
805 control RNAi or *sams-1(RNAi)* or *sams-4(RNAi)* at 37°C. **(F)** Bubble chart showing
806 enriched gene categories in differential peaks as determined by WormCat in animals
807 fed control RNAi at 15°C only, 37°C only and common between 15°C and 37°C (**G**) or
808 *sams-1(RNAi)* and *sams-4(RNAi)* at 37°C. Aggregation plots showing TSS enrichment
809 of Control peaks that did not change after *sams-1(RNAi)* and *sams-4(RNAi)*
810 (independent) **(H)** 15°C or **(I)** 37°C. Shaded areas in the Venn diagrams indicate the
811 population of genes used for plotting the TSS enrichment plots. Aggregation plots
812 showing TSS enrichment of Control peaks that were dependent on *sams-1(RNAi)* or

813 *sams-4(RNAi)* **(J)** 15°C or **(K)** 37°C. Shaded areas in the Venn diagrams indicate the
814 population of genes used for plotting the TSS enrichment plots.
815
816 **Figure 4 Distinct gene expression and H3K4me3 patterns after heat shock in**
817 ***sams-1* and *sams-4* RNAi animals**
818 **(A)** Venn diagram showing overlap of genes upregulated by heat shock in control,
819 *sams-1* or *sams-4* RNAi animals. *sams-1* data is from Ding, et al. 2018. **(B)** Bubble
820 charts show broad category enrichment of up genes determined by Worm-Cat in control
821 (RNAi) or *sams-1* or *sams-4* animals in genes changed (FDR<0.01) after heat shock.
822 **(C)** Heat map for heat shock response genes up regulated following heat shock in
823 animals fed control RNAi, *sams-1* or *sams-4(RNAi).* TSS plots showing aggregation of
824 H3K4me3 in genes upregulated in control, *sams-1* or *sams-4* RNAi at **(D)** 15°C or **(E)**
825 37°C. TSS plots showing aggregation of H3K4me3 in all genes upregulated in control or
826 *sams-1* dependent or *sams-4* RNAi dependent at **(F)** 15°C or **(G)** 37°C. The Y axis on
827 TSS plots shows Peaks per base pair of gene. Genome browser tracks for **(H)** *fbxa-59*
828 and **(I)** *T27F6.8* to visualize changes in H3K4me3 enrichment in animals fed control,
829 *sams-1* or *sams-4(RNAi)* at 15°C or 37°C.
830
831 **Figure 5 Genes that depend on *sams-1* or *sams-4* for expression have reduced**
832 **H3K4me3**
833 **(A)** Venn diagram showing overlap in down regulated genes in animals fed control,
834 *sams-1* or *sams-4(RNAi)* at 37°C. **(B)** Bubble charts show broad category enrichment of
835 metabolism genes determined by Worm-Cat in *sams-1* or *sams-4* animals in genes

836 changed (FDR<0.01) after heat shock. **(C)** Bubble charts show broad category
837 enrichment of transcription factor and metabolism genes determined by Worm-Cat in
838 *sams-1* or *sams-4* animals in genes changed (FDR<0.01) after heat shock. Aggregation
839 plots showing average enrichment of reads around the transcription start site (TSS) in
840 animals fed **(D)** control, **(E)** *sams-1* or **(F)** *sams-4(RNAi)* at 15°C or 37°C. The Y axis on
841 TSS plots shows Peaks per base pair of gene.
842
843 **Figure 6 *nhr* and lipid beta oxidation genes lose H3K4me3 after *sams-1* RNAi but**
844 **expression after heat shock**
845 (**A**) Venn diagram showing the overlap between H3K4me3 peaks identified in animals
846 fed control or *sams-1(RNAi)* at 15°C and down regulated genes identified in heat
847 shocked animals fed *sams-1(RNAi*). Heat map for **(B)** nuclear hormone response genes
848 and **(C)** lipid β-oxidation genes down regulated following heat shock in animals fed
849 control RNAi, *sams-1* or *sams-4(RNAi)*. Genes linked to nhr-68 feedback loop[47] are
850 marked in red. **(D)** Genome browser tracks for *nhr-68* to visualize changes in H3K4me3
851 enrichment in animals fed control, *sams-1* or *sams-4(RNAi)* at 15°C or 37°C.
852
853
854 **Supplemental data**
855 **Fig S1: Expression patterns of SAM synthases in adult *C. elegans***
856 **(A)** Comparison of polyA+ RNA levels of SAM synthases with selected other metabolic
857 genes in adult animals from the modEncode data set[24]. **(B)** Representative confocal
858 images of animals expressing RFP::SAMS-1or GFP::SAMS-4. hypodermis is (h),

859 intestine (i) and germline (gl). (**C**) Confocal projections of GFP::SAMS-4 and SAMS-
860 3::mKate subjected to *sams-3* or *sams-4(RNAi)*. (**D**) Absolute quantification of the SAM
861 level in animals fed on control RNAi or sams-*4(RNAi).* The levels are expressed as
862 mM/mg tissue.
863
864 **Figure S2: Distinct patterns of gene expression after *sams-1 or sams-4* RNAi in**
865 **basal conditions**
866 **(A)** Principal component analysis showing overlapping components between genes
867 regulated in *sams-3* and *sams-4(RNAi)* animals. **(B)** Venn diagram showing the overlap
868 in up regulated genes in animals fed *sams-1* or *sams-4(RNAi).* **(C)** Bubble charts show
869 broad category enrichment of up regulated genes in animals fed *sams-1* or *sams-*
870 *4(RNAi).* **(D)** Bubble charts show broad category enrichment of down regulated genes in
871 animals fed *sams-1* or *sams-4(RNAi).* **(E)** Venn diagram showing the overlap in up
872 regulated genes involved in lipid metabolism in animals fed *sams-1* or *sams-4(RNAi).*
873 **(F)** Venn diagram showing the overlap in up regulated genes involved in pathogen
874 stress response in animals fed *sams-1* or *sams-4(RNAi).*
875
876 **Fig S3: *sams-4* is important for survival and H3K4me3 in *sams-1* animals after**
877 **heat shock.**
878 **(A)** Schematic for the heat stress assay. (**B**) Survival assays comparing response to
879 heat in SAM synthase mutants. (**C**) Lifespan assay with *sams-4(RNAi)* animals where
880 *sams-3* may also be targeted. (**D**) Heat shock survival assays showing that genetic loss
881 of *sams-4* limits survival in *sams-1(RNAi)* animals after heat shock. For B-D, statistical

882 significance is shown by Log-rank test. Each graph represents compiled data from 3
883 biologically independent repeats. Data for each replicate is compiled in Table S2. **(E)**
884 Quantification of immunofluorescence imaging of intestinal nuclei stained with HK4me3
885 antibody after heat shock from *sams-4(ok3315); sams-1(RNAi)* animals. Statistical
886 significance was calculated using unpaired Student's t-test. ns= not significant, **** =
887 p<0.0001, *** = p<0.001. Graph represents compiled data from three biologically
888 independent repeats per condition. LC/MS relative quantitation of SAM (**F**), Methionine
889 (**G**) and S-adenosylhomocysteine (SAH) (**H**). Graphs represent 4 independent
890 biological replicates (1-4: red, blue, orange and green) that were normalized for protein
891 levels before quantitating relative levels of metabolites.
892
893 **Figure S4: H3K4me3 demethylases modulate SAM synthase phenotypes**
894 Representative immunofluorescence images and quantitation of intestinal nuclei stained
895 with H3K4me3 specific antibody for *set-2* (**A, D**), *set-16* (**B, E**) and *rbr-2* (**C, F**).
896 Statistical significance was calculated using unpaired Student's t-test. ns= not
897 significant, **** = p<0.0001, *** = p<0.001. Graph represents compiled data from three
898 biologically independent repeats per condition. Heat shock survival assays examining
899 the impact of demethylase knockdown on *sams-1(lof)* animals for *amx-1* (**G**) and *lsd-1*
900 (**H**). Survival was determined by plotting Kaplan-Meier survival plots. Statistical
901 significance is shown by Log-rank test. Each assay represents compiled data from 3
902 biologically independent repeats (**Table S2**).
903
904 **Figure S5: H3K4me3 C&T correlation with published H3K4me3 ChipSeq data.**

905 (**A**) Correlation plots showing r values for C&T replicates. (**B**) Comparison of
906 H3K4me3ChIP seq from modEncode (L3)[38], Pu et al (Adult *glp-1(e2141)*)[41], Wan et al
907 (adult)[40] and our C&T data. (C) IGV browser tracks showing no antibody controls
908 around the pcaf-1 gene, which has been used as positive control for H3K4me3 5 prime
909 peaks in *C. elegans*[12,32].
910
911 **Figure S6. Distinct gene expression and H3K4me3 patterns after heat shock in**
912 ***sams-1* and *sams-4* RNAi animals**
913 Sunburst diagram showing the enriched gene categories in animals fed control RNAi at
914 **(A)** 15ºC or **(B)** 37ºC. Sunburst diagram showing the overall enriched gene categories
915 **(C)** and genes involved in metabolism **(D)** in animals fed *sams-1(RNAi)* at 37ºC.
916 Sunburst diagram showing the overall enriched gene categories **(E)** and genes involved
917 in metabolism **(F)** in animals fed *sams-4(RNAi)* at 37ºC. Aggregation plots showing
918 average enrichment of reads around the transcription start site (TSS) for genes which
919 are *sams-1* dependent only dependent on either *sams-1* or *sams-4* or *sams-4*
920 dependent only at **(G)** 15ºC or **(H)** 37ºC. The Y axis on TSS plots shows Peaks per
921 base pair of gene.
922
923 **Fig S7. SAM synthase-specific patterns H3K4me3 in germline nuclei.**
924 **(A)** Representative immunofluorescence images of H3K4me3 staining in the germline
925 in animals fed on control, *sams-1* or *sams-4(RNAi)*. **(B)** Venn diagrams showing the
926 overlap in H3K4me3 peaks identified on ubiquitously expressed genes in control
927 animals at 15ºC or 37ºC. **(C)** Venn diagrams showing the overlap in H3K4me3 peaks

928 identified on germline specific genes in control animals at 15ºC or 37ºC. Aggregation
929 plots showing average enrichment of reads around the transcription start site (TSS) of
930 **(D)** ubiquitously or **(E)** germline specific or **(F)** intestine specific genes in animals fed
931 control, *sams-1* or *sams-4(RNAi)* at 15ºC. The Y axis on TSS plots shows Peaks per
932 base pair of gene. Aggregation plots showing average enrichment of reads around the
933 transcription start site (TSS) of **(G)** ubiquitously or **(H)** germline specific or **(I)** intestine
934 specific genes in animals fed control, *sams-1* or *sams-4(RNAi)* at 37ºC.
935
936 **Figure S8: *sams-1* and *sams-4* have distinct gene expression patterns after heat**
937 **shock.**
938 (**A**) PCA plot showing groupings of up and down regulated genes from Control, *sams-1*
939 or *sams-4(RNAi)* animals. Survival curves examining heat shock responses after RNAi
940 of T27F6.8 or *fbxa-59*. Survival was determined by plotting Kaplan-Meier survival plots.
941 Statistical significance is shown by Log-rank test. Each assay represents compiled data
942 from 3 biologically independent repeats (**Table S2**).
943
944 **Figure S9: Schematic of potential *nhr-68* module regulation in sams-1 animals.**
945 (**A**) Genome browser tracks for *ges-1* showing H3K4me3 enrichment in animals fed
946 control, *sams-1* or *sams-4(RNAi)* at 15ºC or 37ºC. (**B**) Schematic showing the dynamic
947 changes in the transcription and H3K4me3 landscape in low SAM animals following
948 heat shock.
949

950 **Table S1 (Microsoft Excel File): RNA seq for SAM synthase knockdown in basal**
951 **conditions. Tabs A-C** show *sams-3, sams-4, sams-5 (RNAi)* RNA seq data then **Tabs**
952 **D-F** show WormCat gene enrichment. *sams-1* data is from Ding, et al. 2018. Enriched
953 categories from WormCat. Red color denoted categories with a p value of less than
954 0.01. NS is not significant, NV is no value, RGS is regulated gene set.
955
956 **Table S2 (Microsoft Excel File) Statistics for survival curves.** Each tab contains
957 data for replicate experiments (R1, R2, R3). Statistical information from GraphPad
958 Prism is also included.
959
960 **Table S3 (Microsoft Excel File). Tabs A-F:** Cut and Tag peaks from Control, *sams-1*
961 and *sams-4* RNAi animals at 15 and 37 degrees determined by HOMER. **Tabs G-I:**
962 Enriched categories from WormCat. Color denoted categories with a p value of less
963 than 0.01 NS is not significant, NV is no value, RGS is regulated gene set.
964
965 **Table S4** (**Microsoft Excel File). Limited activation of heat shock response in**
966 ***sams-4* RNAi animals.** Tabs show RNA seq from control (**A**), *sams-1* (**B**) *or sams-4*
967 **(C**) animals subjected to heat shock that was used for comparison with C&T data.
968 Differential genes were identified using Deseq2 in DolphinNext. Data for control and
969 *sams-1* RNAi animals is from Ding, et al 2018. WormCat batch output of two-fold
970 regulated genes for Categories 1, 2 and 3 are in tabs E-G). Highlighting denotes genes
971 with significantly p values. NS is not significant, NV is no value, RGS is regulated gene
972 set.
973

974
975 **References**
976

977 1. Ducker, G.S., and Rabinowitz, J.D. (2016). One-Carbon Metabolism in Health and
978 Disease. Cell Metab *25*. 10.1016/j.cmet.2016.08.009.

979 2. Mato, J.M., Martínez-Chantar, M.L., and Lu, S.C. (2008). Methionine Metabolism and
980 Liver Disease. Annu Rev Nutr *28*, 273 293. 10.1146/annurev.nutr.28.061807.155438.

981 3. Parkhitko, A.A., Jouandin, P., Mohr, S.E., and Perrimon, N. (2019). Methionine
982 metabolism and methyltransferases in the regulation of aging and lifespan extension
983 across species. Aging Cell *18*, e13034. 10.1111/acel.13034.

984 4. Hansen, M.H.A.L.D.A.K.C. (2005). New Genes tied to Endocrine, Metabolic and
985 Dietary Regulation of Lifespan from a *Caenorhabditis elegans* RNAi Screen. Cell *1*, 119
986 128. 10.1016/j.cell.2015.04.005.

987 5. Han, S., and Brunet, A. (2012). Histone methylation makes its mark on longevity.
988 Trends Cell Biol *22*, 42–49. 10.1016/j.tcb.2011.11.001.

989 6. Greer, E.L., Maures, T.J., Hauswirth, A.G., Green, E.M., Leeman, D.S., Maro, G.S.,
990 Han, S., Banko, M.R., Gozani, O., and Brunet, A. (2010). Members of the H3K4
991 trimethylation complex regulate lifespan in a germline-dependent manner in *C. elegans*.
992 Nature *466*, 383 387. 10.1038/nature09195.

993 7. Han, S., Schroeder, E.A., Silva-García, C.G., Hebestreit, K., Mair, W.B., and Brunet,
994 A. (2017). Mono-unsaturated fatty acids link H3K4me3 modifiers to *C. elegans* lifespan.
995 Nature *544*, 185 190. 10.1038/nature21686.

996 8. Ye, C., and Tu, B.P. (2018). Sink into the Epigenome: Histones as Repositories That
997 Influence Cellular Metabolism. Trends Endocrinol Metabolism *29*, 626 637.
998 10.1016/j.tem.2018.06.002.

999 9. Mentch, S.J., Mehrmohamadi, M., Huang, L., Liu, X., Gupta, D., Mattocks, D.,
1000 Gómez Padilla, P., Ables, G., Bamman, M.M., Thalacker-Mercer, A.E., et al. (2015).
1001 Histone Methylation Dynamics and Gene Regulation Occur through the Sensing of One-
1002 Carbon Metabolism. Cell Metab *22*. 10.1016/j.cmet.2015.08.024.

1003 10. Shyh-Chang, N., Locasale, J.W., Lyssiotis, C.A., Zheng, Y., Teo, R.Y.,
1004 Ratanasirintrawoot, S., Zhang, J., Onder, T., Unternaehrer, J.J., Zhu, H., et al. (2013).
1005 Influence of Threonine Metabolism on *S*-Adenosylmethionine and Histone Methylation.
1006 Science *339*, 222 226. 10.1126/science.1226603.

1007 11. Kraus, D., Yang, Q., Kong, D., Banks, A.S., Zhang, L., Rodgers, J.T., Pirinen, E.,
1008 Pulinilkunnil, T.C., Gong, F., Wang, Y., et al. (2014). Nicotinamide N-methyltransferase

1009 knockdown protects against diet-induced obesity. Nature *508*, 258 262.
1010 10.1038/nature13198.

1011 12. Ding, W., Smulan, L.J., Hou, N.S., Taubert, S., Watts, J.L., and Walker, A.K. (2015).
1012 s-Adenosylmethionine Levels Govern Innate Immunity through Distinct Methylation-
1013 Dependent Pathways. Cell Metab *22*, 633 645. 10.1016/j.cmet.2015.07.013.

1014 13. Towbin, B.D., González-Aguilera, C., Sack, R., Gaidatzis, D., Kalck, V., Meister, P.,
1015 Askjaer, P., and Gasser, S.M. (2012). Step-wise methylation of histone H3K9 positions
1016 heterochromatin at the nuclear periphery. Cell *150*, 934 947. 10.1016/j.cell.2012.06.051.

1017 14. Li, S., Swanson, S.K., Gogol, M., Florens, L., Washburn, M.P., Workman, J.L., and
1018 Suganuma, T. (2015). Serine and SAM Responsive Complex SESAME Regulates
1019 Histone Modification Crosstalk by Sensing Cellular Metabolism. Mol Cell *60*, 408 421.
1020 10.1016/j.molcel.2015.09.024.

1021 15. Liu, M., and Pile, L.A. (2017). The Transcriptional Corepressor SIN3 Directly
1022 Regulates Genes Involved in Methionine Catabolism and Affects Histone Methylation,
1023 Linking Epigenetics and Metabolism*. J Biol Chem *292*, 1970–1976.
1024 10.1074/jbc.m116.749754.

1025 16. Hoffert, K.M., Higginbotham, K.S.P., Gibson, J.T., Oehrle, S., and Strome, E.D.
1026 (2019). Mutations in the S-adenosylmethionine Synthetase Genes, SAM1 and SAM2,
1027 Differentially Impact Genome Stability in Saccharomyces cerevisiae. Genetics *213*,
1028 genetics.302435.2019. 10.1534/genetics.119.302435.

1029 17. Maldonado, L.Y., Arsene, D., Mato, J.M., and Lu, S.C. (2018). Methionine
1030 adenosyltransferases in cancers: Mechanisms of dysregulation and implications for
1031 therapy. Exp Biol Med *243*, 107–117. 10.1177/1535370217740860.

1032 18. Mato, J.M., Corrales, F.J., Lu, S.C., and Avila, M.A. (2002). S-Adenosylmethionine:
1033 a control switch that regulates liver function. FASEB Journal *16*, 15 26.

1034 19. Sullivan, M.R., Darnell, A.M., Reilly, M.F., Kunchok, T., Joesch-Cohen, L.,
1035 Rosenberg, D., Ali, A., Rees, M.G., Roth, J.A., Lewis, C.A., et al. (2021). Methionine
1036 synthase is essential for cancer cell proliferation in physiological folate environments.
1037 Nat Metabolism *3*, 1500–1511. 10.1038/s42255-021-00486-5.

1038 20. Harris, T.W., Arnaboldi, V., Cain, S., Chan, J., Chen, W.J., Cho, J., Davis, P., Gao,
1039 S., Grove, C.A., Kishore, R., et al. (2019). WormBase: a modern Model Organism
1040 Information Resource. Nucleic Acids Res *48*, D762–D767. 10.1093/nar/gkz920.

1041 21. Walker, A.K., Jacobs, R.L., Watts, J.L., Rottiers, V., Jiang, K., Finnegan, D.M.,
1042 Shioda, T., Hansen, M., Yang, F., Niebergall, L.J., et al. (2011). A Conserved SREBP-
1043 1/Phosphatidylcholine Feedback Circuit Regulates Lipogenesis in Metazoans. Cell *147*,
1044 840 852. 10.1016/j.cell.2011.09.045.

1045 22. Nadal, E. de, Ammerer, G., and Posas, F. (2011). Controlling gene expression in
1046 response to stress. Nat Rev Genet *12*, 833–845. 10.1038/nrg3055.

1047 23. Ding, W., Higgins, D.P., Yadav, D.K., Godbole, A.A., Pukkila-Worley, R., and
1048 Walker, A.K. (2018). Stress-responsive and metabolic gene regulation are altered in low
1049 S-adenosylmethionine. Plos Genet *14*, e1007812. 10.1371/journal.pgen.1007812.

1050 24. Gerstein, M.B., Lu, Z.J., Nostrand, E.L.V., Cheng, C., Arshinoff, B.I., Liu, T., Yip,
1051 K.Y., Robilotto, R., Rechtsteiner, A., Ikegami, K., et al. (2010). Integrative analysis of the
1052 Caenorhabditis elegans genome by the modENCODE project. Science *330*, 1775 1787.
1053 10.1126/science.1196914.

1054 25. Kaletsky, R., Yao, V., Williams, A., Runnels, A.M., Tadych, A., Zhou, S.,
1055 Troyanskaya, O.G., and Murphy, C.T. (2018). Transcriptome analysis of adult
1056 Caenorhabditis elegans cells reveals tissue-specific gene and isoform expression. Plos
1057 Genet *14*, e1007559. 10.1371/journal.pgen.1007559.

1058 26. McGhee, J. (2007). The C. elegans intestine. Wormbook, 1–36.
1059 10.1895/wormbook.1.133.1.

1060 27. Holdorf, A.D., Higgins, D.P., Hart, A.C., Boag, P.R., Pazour, G.J., Walhout, A.J.M.,
1061 and Walker, A.K. (2019). WormCat: An Online Tool for Annotation and Visualization of
1062 *Caenorhabditis* elegans Genome-Scale Data. Genetics, genetics.302919.2019.
1063 10.1534/genetics.119.302919.

1064 28. Ye, C., Sutter, B.M., Wang, Y., Kuang, Z., and Tu, B.P. (2017). A Metabolic
1065 Function for Phospholipid and Histone Methylation. Mol Cell *66*, 180 193.e8.
1066 10.1016/j.molcel.2017.02.026.

1067 29. Bannister, A.J., and Kouzarides, T. (2011). Regulation of chromatin by histone
1068 modifications. Cell Res *21*, 381–395. 10.1038/cr.2011.22.

1069 30. Shilatifard, A. (2012). The COMPASS family of histone H3K4 methylases:
1070 mechanisms of regulation in development and disease pathogenesis. Annu Rev
1071 Biochem *81*, 65 95. 10.1146/annurev-biochem-051710-134100.

1072 31. Li, T., and Kelly, W.G. (2011). A role for Set1/MLL-related components in epigenetic
1073 regulation of the *Caenorhabditis elegans* germ line. Plos Genet *7*, e1001349.
1074 10.1371/journal.pgen.1001349.

1075 32. Xiao, Y., Bedet, C., Robert, V.J.P., Simonet, T., Dunkelbarger, S., Rakotomalala, C.,
1076 Soete, G., Korswagen, H.C., Strome, S., and Palladino, F. (2011). *Caenorhabditis*
1077 *elegans* chromatin-associated proteins SET-2 and ASH-2 are differentially required for
1078 histone H3 Lys 4 methylation in embryos and adult germ cells. Proc National Acad Sci
1079 *108*, 8305 8310. 10.1073/pnas.1019290108.

1080 33. Wenzel, D., Palladino, F., and Jedrusik-Bode, M. (2011). Epigenetics in *C. elegans*:
1081 facts and challenges. Genesis *49*, 647 661. 10.1002/dvg.20762.

1082 34. Eissenberg, J.C., and Shilatifard, A. (2010). Histone H3 lysine 4 (H3K4) methylation
1083 in development and differentiation. Dev Biol *339*, 240 249. 10.1016/j.ydbio.2009.08.017.

1084 35. Kaya-Okur, H.S., Wu, S.J., Codomo, C.A., Pledger, E.S., Bryson, T.D., Henikoff,
1085 J.G., Ahmad, K., and Henikoff, S. (2019). CUT&Tag for efficient epigenomic profiling of
1086 small samples and single cells. Nat Commun *10*, 1930. 10.1038/s41467-019-09982-5.

1087 36. Heinz, S., Benner, C., Spann, N., Bertolino, E., Lin, Y.C., Laslo, P., Cheng, J.X.,
1088 Murre, C., Singh, H., and Glass, C.K. (2010). Simple Combinations of Lineage-
1089 Determining Transcription Factors Prime cis-Regulatory Elements Required for
1090 Macrophage and B Cell Identities. Mol Cell *38*, 576–589. 10.1016/j.molcel.2010.05.004.

1091 37. Zhu, L.J., Gazin, C., Lawson, N.D., Pagès, H., Lin, S.M., Lapointe, D.S., and Green,
1092 M.R. (2010). ChIPpeakAnno: a Bioconductor package to annotate ChIP-seq and ChIP-
1093 chip data. Bmc Bioinformatics *11*, 237–237. 10.1186/1471-2105-11-237.

1094 38. Ho, J.W.K., Jung, Y.L., Liu, T., Alver, B.H., Lee, S., Ikegami, K., Sohn, K.-A.,
1095 Minoda, A., Tolstorukov, M.Y., Appert, A., et al. (2014). Comparative analysis of
1096 metazoan chromatin organization. Nature *512*, 449 452. 10.1038/nature13415.

1097 39. Pu, M., Ni, Z., Wang, M., Wang, X., Wood, J.G., Helfand, S.L., Yu, H., and Lee, S.S.
1098 (2015). Trimethylation of Lys36 on H3 restricts gene expression change during aging
1099 and impacts life span. Gene Dev *29*, 718 731. 10.1101/gad.254144.114.

1100 40. Wan, Q.-L., Meng, X., Wang, C., Dai, W., Luo, Z., Yin, Z., Ju, Z., Fu, X., Yang, J.,
1101 Ye, Q., et al. (2022). Histone H3K4me3 modification is a transgenerational epigenetic
1102 signal for lipid metabolism in *Caenorhabditis elegans*. Nat Commun *13*, 768.
1103 10.1038/s41467-022-28469-4.

1104 41. Pu, M., Wang, M., Wang, W., Velayudhan, S.S., and Lee, S.S. (2018). Unique
1105 patterns of trimethylation of histone H3 lysine 4 are prone to changes during aging in
1106 *Caenorhabditis elegans* somatic cells. Plos Genet *14*, e1007466.
1107 10.1371/journal.pgen.1007466.

1108 42. Serizay, J., Dong, Y., Janes, J., Chesney, M., Cerrato, C., and Ahringer, J. (2020).
1109 Distinctive regulatory architectures of germline-active and somatic genes in C. elegans.
1110 Genome Res, gr.265934.120. 10.1101/gr.265934.120.

1111 43. Weiner, A., Chen, H.V., Liu, C.L., Rahat, A., Klien, A., Soares, L., Gudipati, M.,
1112 Pfeffner, J., Regev, A., Buratowski, S., et al. (2012). Systematic dissection of roles for
1113 chromatin regulators in a yeast stress response. Plos Biol *10*, e1001369.
1114 10.1371/journal.pbio.1001369.

1115 44. Morimoto, R.I. (2006). Stress, Aging, and Neurodegenerative Disease. New Engl J
1116 Medicine *355*, 2254–2255. 10.1056/nejmcibr065573.

1117 45. Mahat, D.B., Salamanca, H.H., Duarte, F.M., Danko, C.G., and Lis, J.T. (2016).
1118 Mammalian Heat Shock Response and Mechanisms Underlying Its Genome-wide
1119 Transcriptional Regulation. Mol Cell *62*, 63 78. 10.1016/j.molcel.2016.02.025.

1120 46. Arda, H.E., Taubert, S., MacNeil, L.T., Conine, C.C., Tsuda, B., Gilst, M.V.,
1121 Sequerra, R., Doucette-Stamm, L., Yamamoto, K.R., and Walhout, A.J.M. (2010).
1122 Functional modularity of nuclear hormone receptors in a *Caenorhabditis elegans*
1123 metabolic gene regulatory network. Mol Syst Biol *6*, 367. 10.1038/msb.2010.23.

1124 47. Bulcha, J.T., Giese, G.E., Ali, Md.Z., Lee, Y.-U., Walker, M.D., Holdorf, A.D., Yilmaz,
1125 L.S., Brewster, R.C., and Walhout, A.J.M. (2019). A Persistence Detector for Metabolic
1126 Network Rewiring in an Animal. Cell Reports *26*, 460-468.e4.
1127 10.1016/j.celrep.2018.12.064.

1128 48. Cheng, C., and Kurdistani, S.K. (2022). Chromatin as a metabolic organelle:
1129 Integrating the cellular flow of carbon with gene expression. Mol Cell *82*, 8–9.
1130 10.1016/j.molcel.2021.12.003.

1131 49. Hsieh, W.-C., Sutter, B.M., Ruess, H., Barnes, S.D., Malladi, V.S., and Tu, B.P.
1132 (2022). Glucose starvation induces a switch in the histone acetylome for activation of
1133 gluconeogenic and fat metabolism genes. Mol Cell *82*, 60-74.e5.
1134 10.1016/j.molcel.2021.12.015.

1135 50. Wellen, K.E., Hatzivassiliou, G., Sachdeva, U.M., Bui, T.V., Cross, J.R., and
1136 Thompson, C.B. (2009). ATP-Citrate Lyase Links Cellular Metabolism to Histone
1137 Acetylation. Science *324*, 1076 1080. 10.1126/science.1164097.

1138 51. Mentch, S.J., and Locasale, J.W. (2016). One-carbon metabolism and epigenetics:
1139 understanding the specificity. Ann Ny Acad Sci *1363*, 91 98. 10.1111/nyas.12956.

1140 52. Walsh, C.T., Tu, B.P., and Tang, Y. (2017). Eight Kinetically Stable but
1141 Thermodynamically Activated Molecules that Power Cell Metabolism. Chem Rev *118*,
1142 acs.chemrev.7b00510. 10.1021/acs.chemrev.7b00510.

1143 53. Lu, S.C., Alvarez, L., Huang, Z.-Z., Chen, L., An, W., Corrales, F.J., Avila, M.A.,
1144 Kanel, G., and Mato, J.M. (2001). Methionine adenosyltransferase 1A knockout mice
1145 are predisposed to liver injury and exhibit increased expression of genes involved in
1146 proliferation. Proc National Acad Sci *98*, 5560–5565. 10.1073/pnas.091016398.

1147 54. Annibal, A., Tharyan, R.G., Schonewolff, M.F., Tam, H., Latza, C., Auler, M.M.K.,
1148 Grönke, S., Partridge, L., and Antebi, A. (2021). Regulation of the one carbon folate
1149 cycle as a shared metabolic signature of longevity. Nat Commun *12*, 3486.
1150 10.1038/s41467-021-23856-9.

1151 55. Gao, X., Sanderson, S.M., Dai, Z., Reid, M.A., Cooper, D.E., Lu, M., Richie, J.P.,
1152 Ciccarella, A., Calcagnotto, A., Mikhael, P.G., et al. (2019). Dietary methionine links
1153 nutrition and metabolism to the efficacy of cancer therapies. Nature *572*, 397–401.
1154 10.1038/s41586-019-1437-3.

1155 56. Sun, Y., and Locasale, J.W. (2021). Rethinking the bioavailability and cellular
1156 transport properties of S-adenosylmethionine. Cell Stress *6*, 1–5.
1157 10.15698/cst2022.01.261.

1158 57. Tang, S., Fang, Y., Huang, G., Xu, X., Padilla-Banks, E., Fan, W., Xu, Q.,
1159 Sanderson, S.M., Foley, J.F., Dowdy, S., et al. (2017). Methionine metabolism is
1160 essential for SIRT1-regulated mouse embryonic stem cell maintenance and embryonic
1161 development. Embo J *36*, 3175–3193. 10.15252/embj.201796708.

1162 58. Dai, Z., Mentch, S.J., Gao, X., Nichenametla, S.N., and Locasale, J.W. (2018).
1163 Methionine metabolism influences genomic architecture and gene expression through
1164 H3K4me3 peak width. Nat Commun *9*, 1955. 10.1038/s41467-018-04426-y.

1165 59. Murray, B., Barbier-Torres, L., Fan, W., Mato, J.M., and Lu, S.C. (2019). Methionine
1166 adenosyltransferases in liver cancer. World J Gastroentero *25*, 4300–4319.
1167 10.3748/wjg.v25.i31.4300.

1168 60. Greco, C.M., Cervantes, M., Fustin, J.-M., Ito, K., Ceglia, N., Samad, M., Shi, J.,
1169 Koronowski, K.B., Forne, I., Ranjit, S., et al. (2020). S-adenosyl-l-homocysteine
1170 hydrolase links methionine metabolism to the circadian clock and chromatin remodeling.
1171 Sci Adv *6*, eabc5629. 10.1126/sciadv.abc5629.

1172 61. Hödl, M., and Basler, K. (2012). Transcription in the Absence of Histone H3.2 and
1173 H3K4 Methylation. Curr Biol *22*, 2253 2257. 10.1016/j.cub.2012.10.008.

1174 62. Das, S., Min, S., and Prahlad, V. (2021). Gene bookmarking by the heat shock
1175 transcription factor programs the insulin-like signaling pathway. Mol Cell *81*, 4843-
1176 4860.e8. 10.1016/j.molcel.2021.09.022.

1177 63. Yukselen, O., Turkyilmaz, O., Ozturk, A.R., Garber, M., and Kucukural, A. (2020).
1178 DolphinNext: a distributed data processing platform for high throughput genomics. Bmc
1179 Genomics *21*, 310. 10.1186/s12864-020-6714-x.

1180 64. Kucukural, A., Yukselen, O., Ozata, D.M., Moore, M.J., and Garber, M. (2019).
1181 DEBrowser: interactive differential expression analysis and visualization tool for count
1182 data. Bmc Genomics *20*, 6. 10.1186/s12864-018-5362-x.

1183 65. Hulsen, T., Vlieg, J. de, and Alkema, W. (2008). BioVenn – a web application for the
1184 comparison and visualization of biological lists using area-proportional Venn diagrams.
1185 Bmc Genomics *9*, 488. 10.1186/1471-2164-9-488.

1186 66. Higgins, D.P., Weisman, C.M., Lui, D.S., D'Agostino, F.A., and Walker, A.K. (2022).
1187 Defining characteristics and conservation of poorly annotated genes in *Caenorhabditis*
1188 *elegans* using WormCat 2.0. Genetics. 10.1093/genetics/iyac085.

1189 67. Kaya-Okur, H.S., Wu, S.J., Codomo, C.A., Pledger, E.S., Bryson, T.D., Henikoff,
1190 J.G., Ahmad, K., and Henikoff, S. (2019). CUT&Tag for efficient epigenomic profiling of
1191 small samples and single cells. Nat Commun *10*, 1930. 10.1038/s41467-019-09982-5.

1192 68. Langmead, B., Trapnell, C., Pop, M., and Salzberg, S.L. (2009). Ultrafast and
1193 memory-efficient alignment of short DNA sequences to the human genome. Genome
1194 Biol *10*, R25–R25. 10.1186/gb-2009-10-3-r25.

1195 69. Ramírez, F., Ryan, D.P., Grüning, B., Bhardwaj, V., Kilpert, F., Richter, A.S., Heyne,
1196 S., Dündar, F., and Manke, T. (2016). deepTools2: a next generation web server for
1197 deep-sequencing data analysis. Nucleic Acids Res *44*, W160–W165.
1198 10.1093/nar/gkw257.

1199

1200

Godbole et al
Figure 1

A

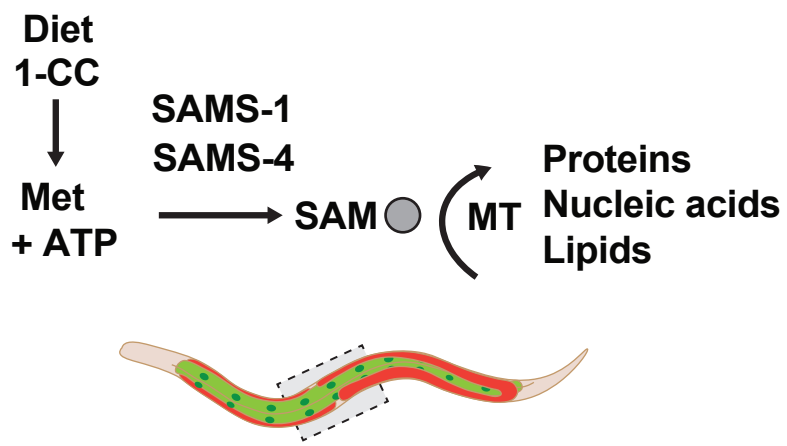

B

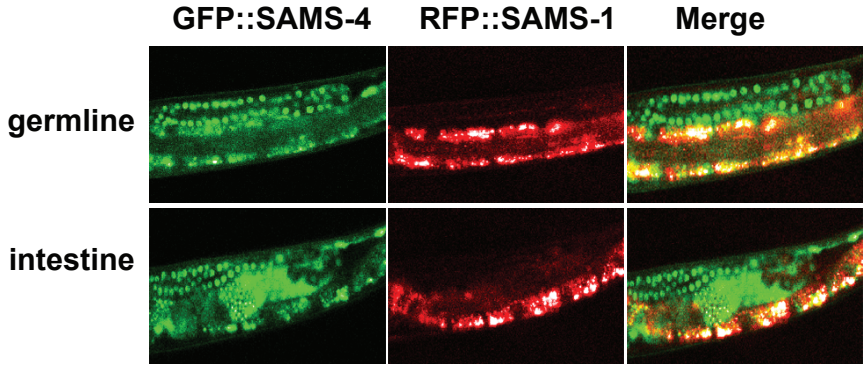

C

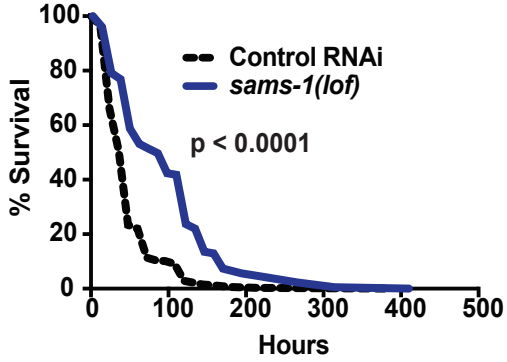

D

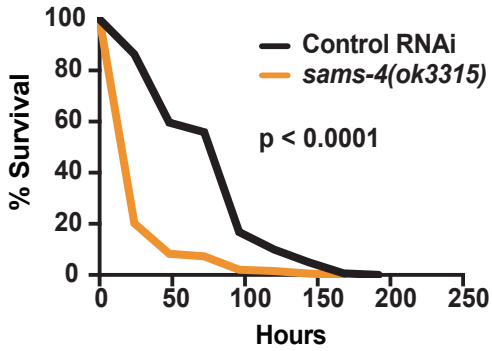

E

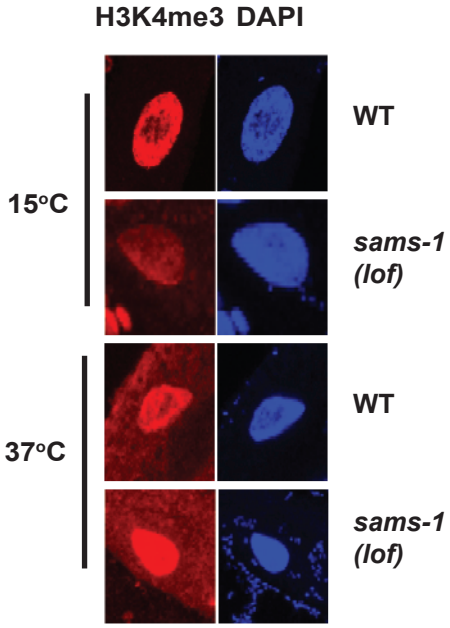

F

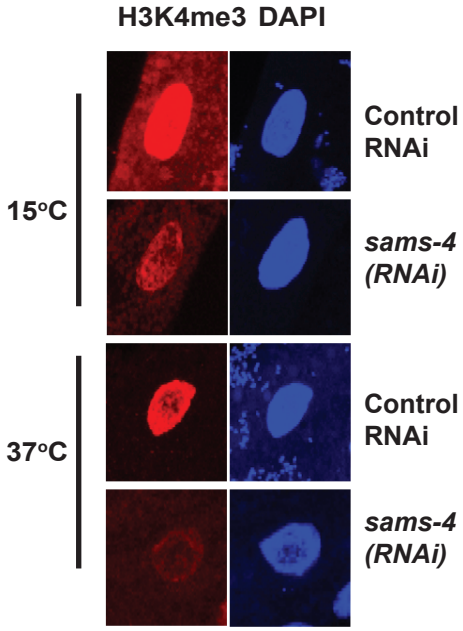

G

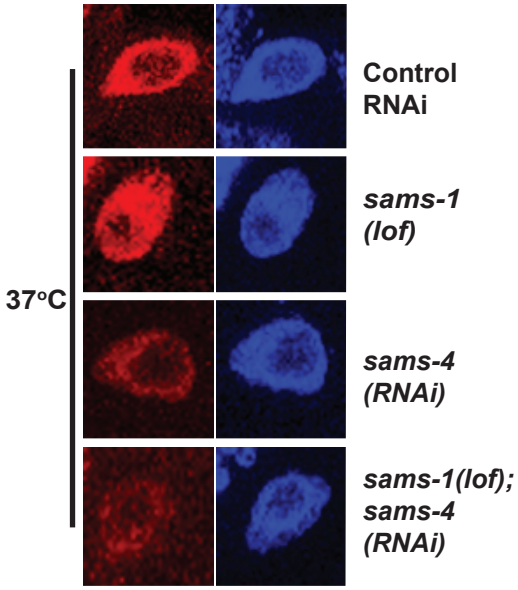

H

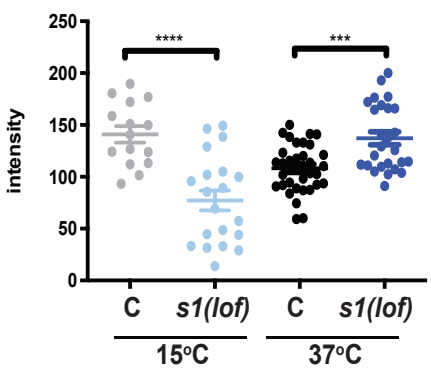

I

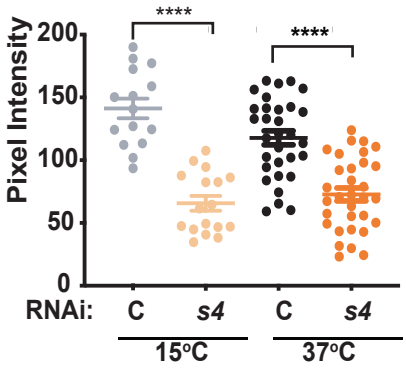

J

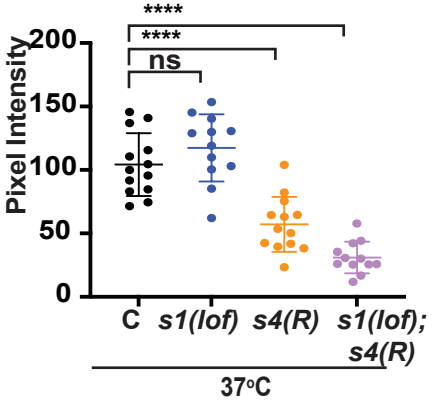

Godbole, et al.
Figure 2

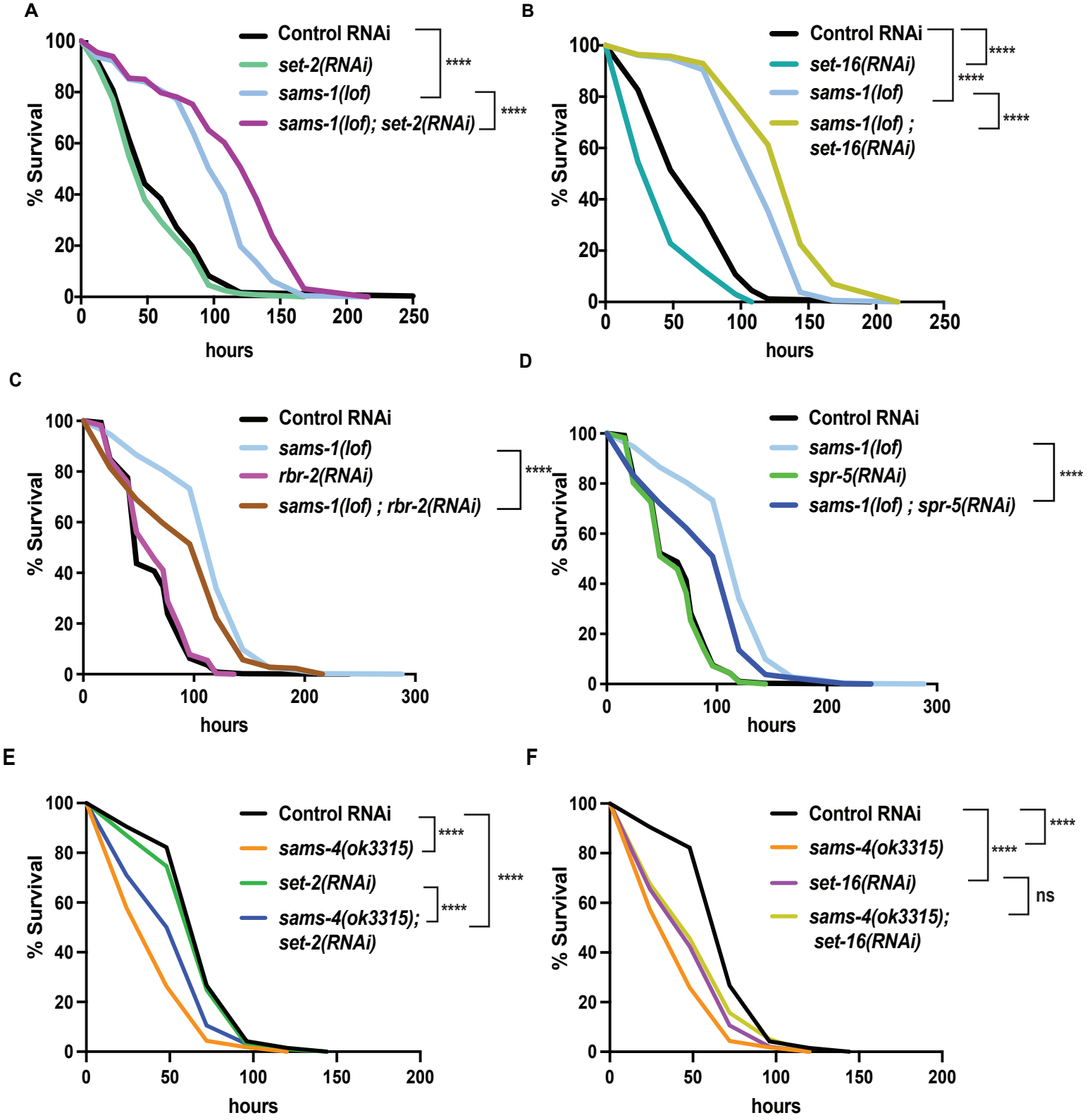

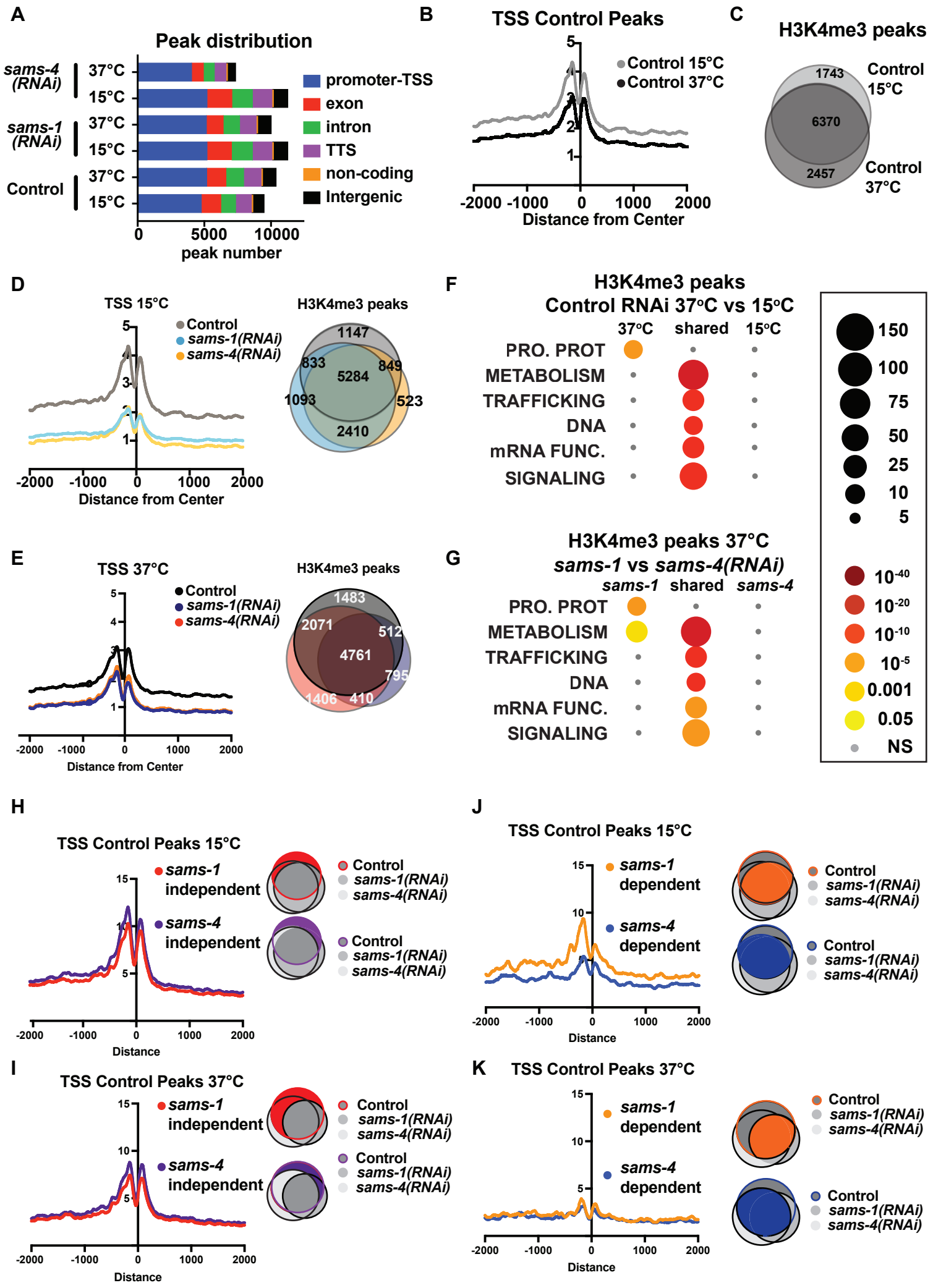
A
Peak distribution
sams-4 (RNAi)
37°C
15°C
sams-1 (RNAi)
37°C
15°C
Control
37°C
15°C
promoter-TSS
exon
intron
TTS
non-coding
Intergenic
0
5000
10000
peak number
B
TSS Control Peaks
Control 15°C
Control 37°C
-2000 -1000 0 1000 2000
Distance from Center
C
H3K4me3 peaks
1743
6370
2457
Control 15°C
Control 37°C
D
TSS 15°C
Control
sams-1(RNAi)
sams-4(RNAi)
-2000 -1000 0 1000 2000
Distance from Center
H3K4me3 peaks
1147
833
849
5284
1093
523
2410
E
TSS 37°C
Control
sams-1(RNAi)
sams-4(RNAi)
-2000 -1000 0 1000 2000
Distance from Center
H3K4me3 peaks
1483
2071
512
4761
795
1406
410
F
H3K4me3 peaks
Control RNAi 37°C vs 15°C
37°C
shared
15°C
PRO. PROT
METABOLISM
TRAFFICKING
DNA
mRNA FUNC.
SIGNALING
150
100
75
50
25
10
5
10-40
10-20
10-10
10-5
0.001
0.05
NS
G
H3K4me3 peaks 37°C
sams-1 vs sams-4(RNAi)
sams-1
shared
sams-4
PRO. PROT
METABOLISM
TRAFFICKING
DNA
mRNA FUNC.
SIGNALING
H
TSS Control Peaks 15°C
sams-1 independent
sams-4 independent
Control
sams-1(RNAi)
sams-4(RNAi)
-2000 -1000 0 1000 2000
Distance
I
TSS Control Peaks 37°C
sams-1 independent
sams-4 independent
Control
sams-1(RNAi)
sams-4(RNAi)
-2000 -1000 0 1000 2000
Distance
J
TSS Control Peaks 15°C
sams-1 dependent
sams-4 dependent
Control
sams-1(RNAi)
sams-4(RNAi)
-2000 -1000 0 1000 2000
Distance
K
TSS Control Peaks 37°C
sams-1 dependent
sams-4 dependent
Control
sams-1(RNAi)
sams-4(RNAi)
-2000 -1000 0 1000 2000
Distance

Godbole et al
Figure 4

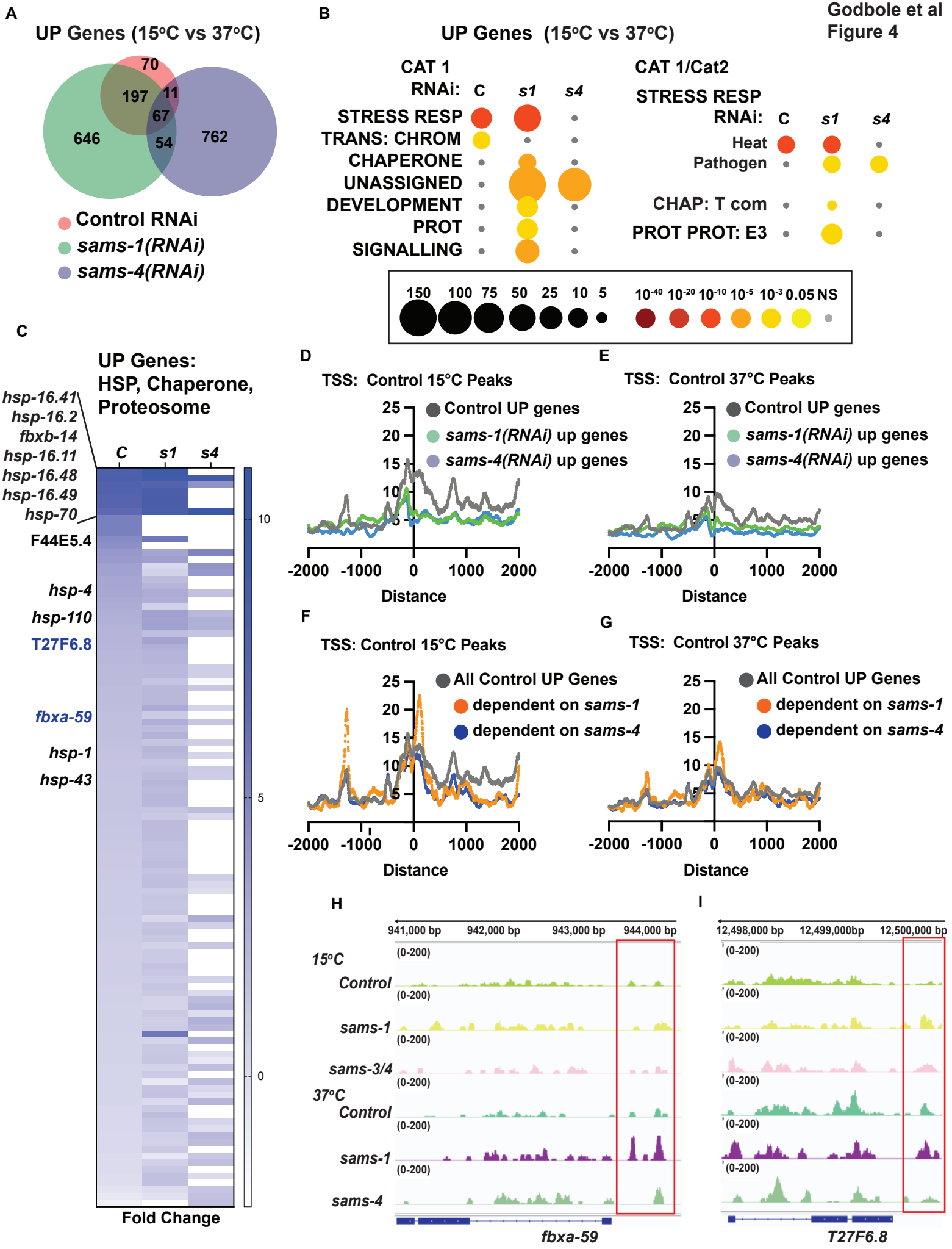

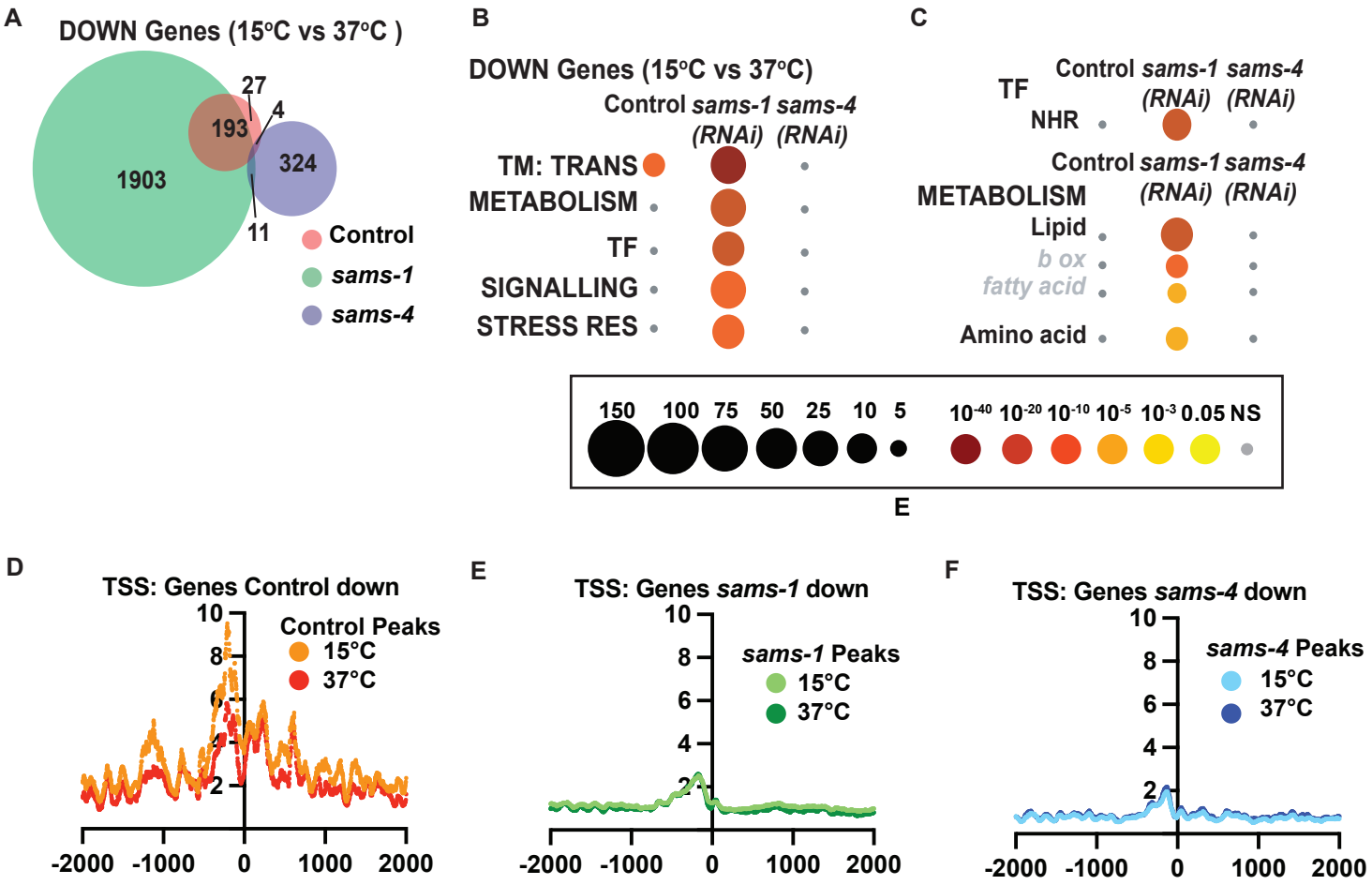
A
DOWN Genes (15°C vs 37°C)
1903
193
27
4
324
11
Control
sams-1
sams-4
B
DOWN Genes (15°C vs 37°C)
Control sams-1 (RNAi) sams-4 (RNAi)
TM: TRANS
METABOLISM
TF
SIGNALLING
STRESS RES
C
TF
NHR
Control sams-1 (RNAi) sams-4 (RNAi)
METABOLISM
Lipid
b ox
fatty acid
Amino acid
150 100 75 50 25 10 5
10-40 10-20 10-10 10-5 10-3 0.05 NS
E
D
TSS: Genes Control down
Control Peaks
15°C
37°C
-2000 -1000 0 1000 2000
E
TSS: Genes sams-1 down
sams-1 Peaks
15°C
37°C
-2000 -1000 0 1000 2000
F
TSS: Genes sams-4 down
sams-4 Peaks
15°C
37°C
-2000 -1000 0 1000 2000

A

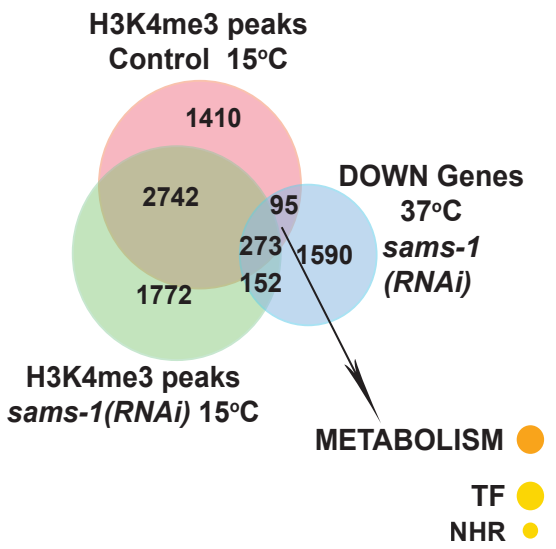
H3K4me3 peaks
Control 15°C
1410
2742
95
273
1590
152
1772
DOWN Genes
37°C
sams-1
(RNAi)
H3K4me3 peaks
sams-1(RNAi) 15°C
METABOLISM
TF
NHR

B

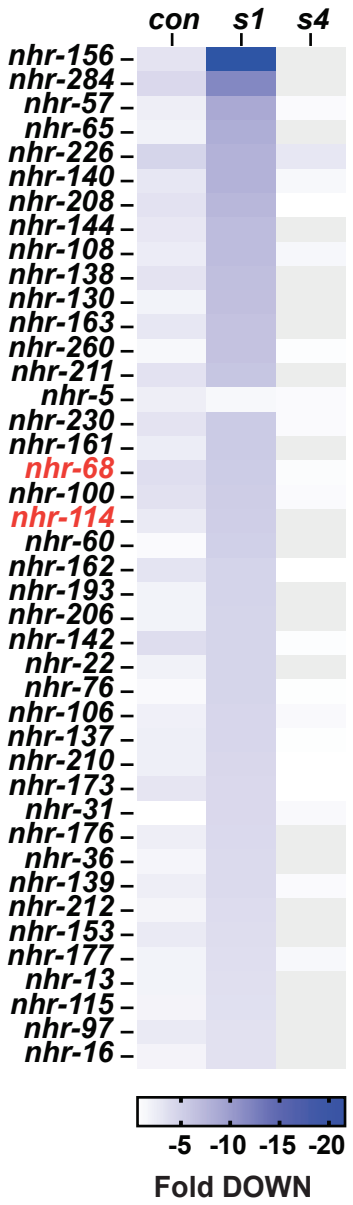
con
s1
s4
nhr-156
nhr-284
nhr-57
nhr-65
nhr-226
nhr-140
nhr-208
nhr-144
nhr-108
nhr-138
nhr-130
nhr-163
nhr-260
nhr-211
nhr-5
nhr-230
nhr-161
nhr-68
nhr-100
nhr-114
nhr-60
nhr-162
nhr-193
nhr-206
nhr-142
nhr-22
nhr-76
nhr-106
nhr-137
nhr-210
nhr-173
nhr-31
nhr-176
nhr-36
nhr-139
nhr-212
nhr-153
nhr-177
nhr-13
nhr-115
nhr-97
nhr-16
-5 -10 -15 -20
Fold DOWN

C

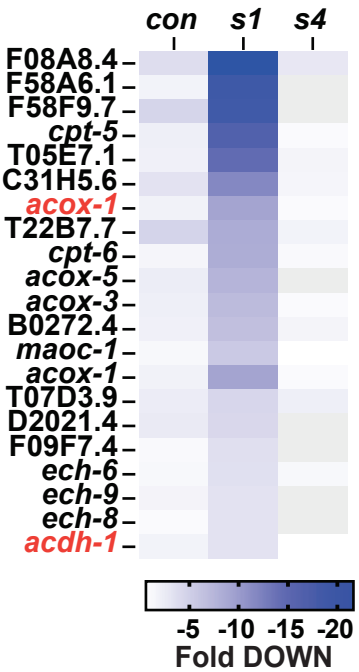
con
s1
s4
F08A8.4
F58A6.1
F58F9.7
cpt-5
T05E7.1
C31H5.6
acox-1
T22B7.7
cpt-6
acox-5
acox-3
B0272.4
maoc-1
acox-1
T07D3.9
D2021.4
F09F7.4
ech-6
ech-9
ech-8
acdh-1
-5 -10 -15 -20
Fold DOWN

D

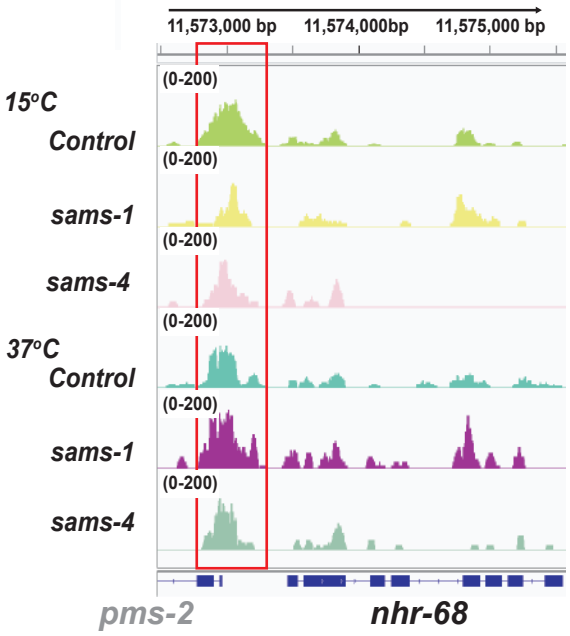
11,573,000 bp
11,574,000bp
11,575,000 bp
15°C
Control
sams-1
sams-4
37°C
Control
sams-1
sams-4
(0-200)
pms-2
nhr-68

E

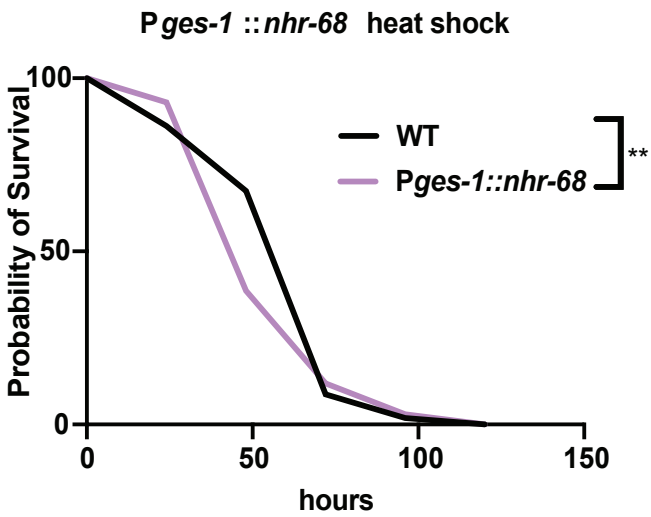
Pges-1 ::nhr-68 heat shock
Probability of Survival
100
50
0
WT
Pges-1::nhr-68
**
0
50
100
150
hours